PHOTOCHROMIC MATERIALS RESEARCH FOR OPTICAL DISPLAY

R. C. Duncan
RCA Laboratories
Princeton, New Jersey 08540

May 1971
Final Report for Period 1 June 1970 – 31 January 1971

Prepared for
Goddard Space Flight Center
Greenbelt, Maryland 20771

Requests for copies of this report should be referred to

National Aeronautics and Space Administration
Office of Scientific and Technical Information
Attention: AFSS-A
Washington, D.C. 20546

1. Report No.	2. Government Accession No.	3. Recipient's Catalog No.
Final		

4. Title and Subtitle	5. Report Date
Photochromic Materials Research for Optical Display	May 1971
	6. Performing Organization Code
7. Author(s) R. C. Duncan	8. Performing Organization Report No.
9. Performing Organization Name and Address RCA Laboratories Princeton, New Jersey 08540	10. Work Unit No.
	11. Contract or Grant No. NAS 5-10335
12. Sponsoring Agency Name and Address Goddard Space Flight Center Greenbelt, Maryland 20771	13. Type of Report and Period Covered Final Report 1 June 1970 through 31 January 1971
	14. Sponsoring Agency Code

15. Supplementary Notes

16. Abstract

We have carried out an extensive quantitative and comparative evaluation of a broad range of state-of-the-art inorganic photochromic materials that offer potential as information input planes for coherent optical data-processing applications. The evaluated samples comprise 17 wafers of various thicknesses of CaF_2:La,Na; CaF_2:Ce,Na; $SrTiO_3$:Ni,Mo,Al; and $CaTiO_3$:Ni,Mo. The range of wafer thicknesses included is 0.13 to 1.02 mm. The evaluation includes consideration of available wafer size and crystal quality, photochromic absorption spectra, quantitative erase-mode sensitometry, time-intensity reciprocity, and resolution capabilities. Most of the evaluative tests were carried out in the erase mode using coherent 5145 Å argon laser radiation. The results of these tests are presented and summarized in numerous graphs, tables, and photographs distributed throughout the text and in three appendices. Some very general characteristics of the several materials evaluated are very briefly summarized below. A. CaF_2 (with La, Na or Ce, Na dopants: (1) Very high optical quality; (2) Moderately large wafer sizes available; (3) Long photochromic lifetime; (4) Excellent time-intensity reciprocity in the erase mode; (5) Relatively low erase mode sensitivity; (6) Low photochromic optical density per unit wafer thickness; (7) Moderate resolution capability, but at low contrast. B. $SrTiO_3$:Ni,Mo,Al: (1) Large wafer sizes available; (2) Moderate to good optical quality; (3) Relatively high erase mode sensitivity; (4) High photochromic optical density per unit wafer thickness; (5) Good resolution capability; (6) Short photochromic thermal lifetime; (7) Poor time-intensity reciprocity in the erase mode. C. $CaTiO_3$:Ni,Mo: (1) High photochromic optical density per unit wafer thickness; (2) Moderate photochromic thermal lifetime; (3) Good resolution capability, but seriously limited by poor optical quality; (4) Relatively poor time-intensity reciprocity in the erase mode; (5) Relatively low erase mode sensitivity; (6) Relatively small wafer sizes available; (7) Poor optical quality.

17. Key Words (Selected by Author(s))	18. Distribution Statement
CaF_2:La,Na; CaF_2:Ce,Na; $SrTiO_3$:Ni,Mo,Al; $CaTiO_3$:Ni,Mo; Photochromic absorption spectra; optical quality; sensitivity; resolution.	

19. Security Classif. (of this report)	20. Security Classif. (of this page)	21. No. of Pages	22. Price*
Unclassified	Unclassified	73	

*For sale by the Clearinghouse for Federal Scientific and Technical Information, Springfield, Virginia 22151.

ABSTRACT

We have carried out an extensive quantitative and comparative evaluation of a broad range of state-of-the-art inorganic photochromic materials that offer potential as information input planes for coherent optical data-processing applications. The evaluated samples comprise 17 wafers of various thicknesses of CaF_2:La,Na; CaF_2:Ce,Na; $SrTiO_3$:Ni,Mo,Al; and $CaTiO_3$:Ni,Mo. The range of wafer thicknesses included is 0.13 to 1.02 mm. The evaluation includes consideration of available wafer size and crystal quality, photochromic absorption spectra, quantitative erase mode sensitometry, time-intensity reciprocity, and resolution capabilities. Most of the evaluative tests were carried out in the erase mode using coherent 5145 Å argon laser radiation. The results of these tests are presented and summarized in numerous graphs, tables, and photographs distributed throughout the text and in three appendices.

Some very general characteristics of the several materials evaluated are very briefly summarized below:

A. CaF_2 (WITH La,Na OR Ce,Na DOPANTS)

1. Very high optical quality.
2. Moderately large wafer sizes available.
3. Long photochromic lifetime.
4. Excellent time-intensity reciprocity in the erase mode.
5. Relatively low erase mode sensitivity.
6. Low photochromic optical density per unit wafer thickness.
7. Moderate resolution capability, but at low contrast.

B. $SrTiO_3$:Ni,Mo,Al

1. Large wafer sizes available.
2. Moderate to good optical quality.
3. Relatively high erase mode sensitivity.
4. High photochromic optical density per unit wafer thickness.
5. Good resolution capability.
6. Short photochromic thermal lifetime.
7. Poor time-intensity reciprocity in the erase mode.

C. $CaTiO_3$:Ni,Mo

1. High photochromic optical density per unit wafer thickness.
2. Moderate photochromic thermal lifetime.
3. Good resolution capability, but seriously limited by poor optical quality.
4. Relatively poor time-intensity reciprocity in the erase mode.
5. Relatively low erase mode sensitivity.
6. Relatively small wafer sizes available.
7. Poor optical quality.

TABLE OF CONTENTS

TABLE OF CONTENTS (Continued)

LIST OF ILLUSTRATIONS

LIST OF TABLES

I. INTRODUCTION

The techniques of coherent optical data processing are finding increased use in a variety of information-handling applications. For certain processing operations these techniques permit much faster and more economical data handling than is presently possible by digital methods. In most optical processors the format for information input is that of optical transparencies which impose a two-dimensional spacial modulation of amplitude (or phase) on transmitted coherent light. These transparencies, usually on photographic film, must be pre-recorded and chemically developed, a time-consuming and expensive process which effectively precludes realtime optical processing.

Inorganic single-crystal photochromic materials developed at RCA Laboratories appear to offer significant fundamental advantages over photographic film for the spatial modulation of light in many coherent optical-processing applications. Perhaps most important among these are (1) the possibility of recording the input information without the requirement of post-recording image development - thus making potentially feasible real-time optical image processing, and (2) the eraseability and essentially indefinite reusability of these materials.

Research on these materials over the past few years has focused on the identification of the active photochromic color centers and the understanding and control of the fundamental photochromic mechanisms. Developmental effort, much of it carried out with NASA contract support, has emphasized the attainment of improved photochromic performance through (1) optimum selection of dopants and dopant concentrations, (2) better material preparation and treatment techniques, and (3) elimination or control of competing optical-absorption processes.

One of the purposes of the present contract has been to continue this development program. In particular, efforts have been made to produce greater concentrations of active color centers in photochromic CaF_2, to improve the optical quality of photochromic $CaTiO_3$, and to obtain larger area wafers of photochromic $SrTiO_3$. These efforts are discussed in Section II of this Report.

The second, and perhaps more important, purpose of this contract has been to carry out, for the first time, a quantitative and comparative evaluation of the pertinent photochromic properties of a number of these single-crystal materials which are potentially appropriate for the optical processing application. The evaluation reported here includes (in Sections III through V, respectively) data on the photochromic absorption spectra, erase mode sensitivities to argon laser radiation, the validity of time-intensity reciprocity, and the resolution capabilities of wafer samples of four state-of-the-art materials. Included in this

study were crystal wafers of several different thicknesses of each of these photochromic materials. The basis for the selection of these materials was discussed in the Ninth Progress Report on this contract[1] and is not repeated here.

The results of the evaluation experiments are presented largely in the form of graphs, tables, and photographs. The text of the report summarizes, compares, and interprets these results in only a very general way.

A word should be said here about completeness. Not all of the tests requested by NASA that are appropriate for a complete evaluation have been carried out. Very serious problems were encountered in acquiring and/or preparing satisfactory high-quality state-of-the-art materials for evaluation. A disproportionate amount of time and effort, therefore, was expended in overcoming or trying to overcome these unanticipated difficulties. The nature of these problems and, where applicable, their solutions are discussed in Section II of this report. The resulting delays and diversion of effort away from evaluation experiments were believed to be preferable to a more complete evaluation of samples of particularly poor optical and/or photochromic quality.

All of the wafer samples evaluated under this contract are being forwarded to NASA under separate cover. These samples represent the present state-of-the-art in optical and photochromic quality and wafer size.

II. MATERIALS

General information on each of the photochromic wafer samples tested and evaluated under this contract is shown in Table I. The first two columns list the host crystals, the dopants, and the nominal dopant concentrations of the several crystals from which the various wafers were cut. The basis for the selection of these particular host-dopant combinations was discussed in some detail in the Ninth Progress Report[1] on this contract. Dopant concentrations were chosen to lie within relatively broad ranges found in earlier studies to give maximum photochromic effects[2,3]. The numbers in the third column, identifying both the individual wafers and the crystal boules they came from, will be used throughout this report, some in an abbreviated form, to refer to the specific wafer or wafers under consideration.

It is important to point out that the materials listed in Table I are, as photochromic materials at least, still very much developmental materials. The precise details of the crystal-growth and sample-treatment procedures are not widely known nor completely understood. The photochromic behavior of the crystalline material that results is not entirely controllable or reproducible. These crystals are only available commercially from a very limited number of suppliers, and then only on a "best effort" basis and without specification of the optical and photochromic properties.

The suppliers of the crystals required for test, evaluation, and delivery to NASA under this contract represent the widest experience and greatest expertise available in the growth of the respective photochromic quality crystals. Problems and delays have nevertheless been encountered in obtaining crystals of satisfactory quality. These problems are discussed later in this Section. We believe them to be directly attributable to the developmental nature of these materials.

A. CaF_2

1. Crystals

The photochromic wafers of CaF_2 used in this evaluation came from two single-crystal boules of CaF_2, one La-doped and the other Ce-doped. These crystals were grown by H. E. Temple of RCA Laboratories using a gradient freeze technique developed here a number of years ago by P. G. Herkart and H. E. Temple. Such crystals have been grown on a relatively routine basis at these Laboratories for several years. However, appreciable and unexplained crystal-to-crystal variations in their photochromic quality have never been completely eliminated.

The optical quality of these crystals is generally excellent. This is illustrated by the transmission photomicrographs of wafers 750-2 and

T A B L E I

WAFER SAMPLES TESTED

Host	Dopants	Identification Number	Thickness (mm)
CaF_2	0.05 mol% La 0.1 mol%Na	750-2 750-3 750-4 750-5	0.81 0.53 0.29 0.13
CaF_2	0.05 mol% Ce 0.1 mol% Na	751-1 751-2 751-3	0.86 0.53 0.32
$SrTiO_3$	0.14 wt% NiO 0.26 wt% MoO_3 0.1 wt% Al_2O_3	70L-17-ST-2-0 -ST-2-4 -ST-2-6 -ST-2-10	1.02 0.53 0.28 0.18
$CaTiO_3$	0.3 wt% $NiMoO_4$	70M-2-CT-3A -CT-1 -1 -CT-3C-2 -CT-3C-1	0.81 0.56 0.31 0.18
$CaTiO_3$	0.1 wt% NiO 0.2 wt% MoO_3	70F-16-CT-1 -0 -CT-2C-0	0.51 0.32

751-1 shown in Figure 1. Figures 1(a) and 1(b) show direct transmission through the respective wafers. For Figures 1(c) and 1(d), the respective wafers were placed between crossed polarizers; no strains or optical distortions are visible. The scale of these pictures can be determined from the fact that each wafer is very slightly under 1.0 cm wide.

The largest crystals that can be grown in the present furnace facilities are about 1 cm in diameter and 6 cm long. The optical quality and unwanted impurity level in approximately the last 1 cm of the crystal to solidify are frequently not acceptable. The dopant concentration may vary by as much as a factor of two along the remaining 5 cm or so of the length. In the present work, the crystals were cut parallel to this long dimension in order to provide wafer samples of the desired thickness and of as large an area as possible. Clearly, only two or three wafers from a single boule can come very close to the full 1 x 5 cm maximum possible size. Following additive coloration (see below), each wafer exhibiting satisfactory photochromic properties was optically polished on both sides.

2. ADDITIVE COLORATION

The wafer samples must be additively colored to produce photochromic color centers. This additive coloration (AC) process has been extensively discussed in earlier reports on this contract[4] and elsewhere[2]. It was necessary, in this case as in most others, to separately optimize the controllable parameters of this process for the wafers of each different crystal.

3. PROBLEMS WITH PHOTOCHROMIC QUALITY

The first four CaF_2 crystals grown for test and evaluation under this contract proved to be of exceptionally poor photochromic quality. The dominant AC-induced coloration was a "blotchy" non-photochromic background absorption. This "blotch" is common, though usually to a much lesser extent, to all heavily colored photochromic CaF_2. In this case even lightly colored wafers were "blotched," and no adjustment of the parameters of the AC process brought about any significant improvement.

The subsequent intensive search for the causes of, and a quick "cure" for, this "epidemic" of poor photochromic quality consumed a considerable amount of time and effort during the latter portion of the contract period. Eight additional boules of CaF_2:La,Na or CaF_2:Ce,Na were grown, under a variety of growth and annealing conditions. In addition, the concentrations of La or Ce in the crystals were varied by a factor of two. Wafers cut from each boule were then additively colored also under different conditions.

Wafer 750-2

Wafer 751-1

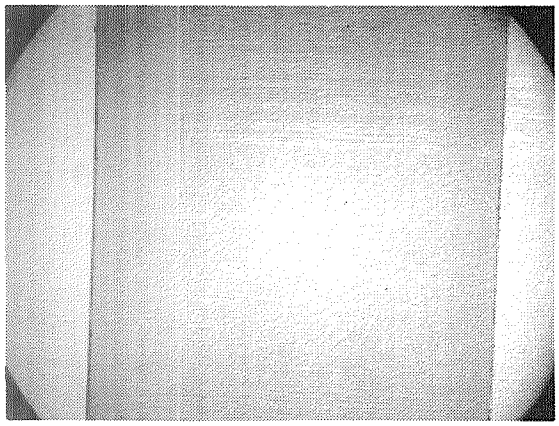

(a)

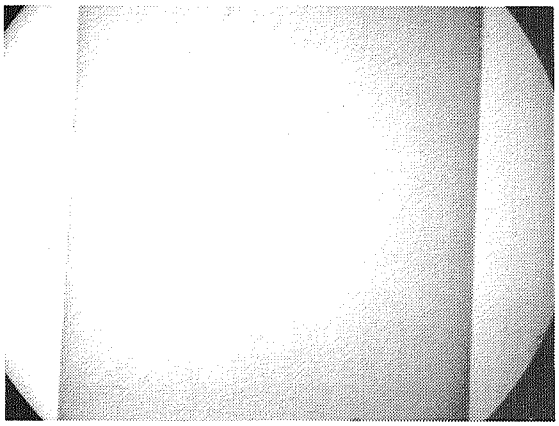

(c)

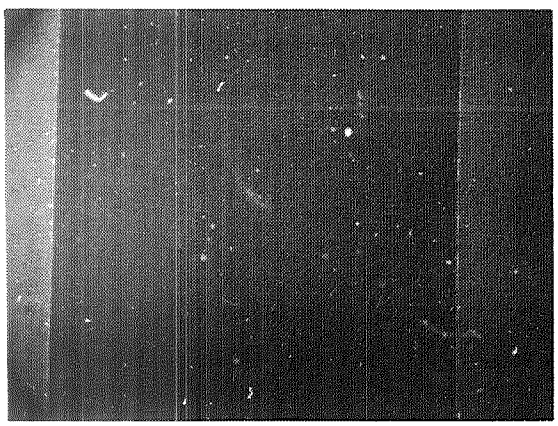

(b)

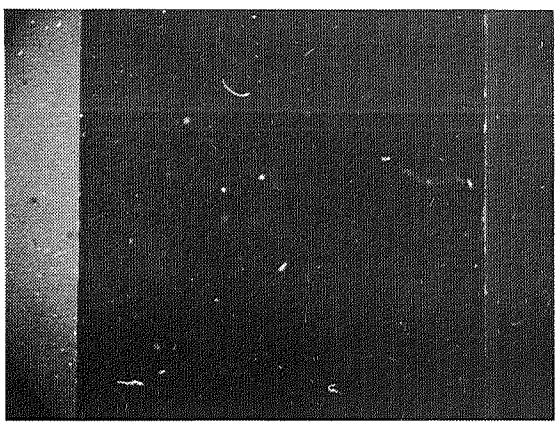

(d)

Figure 1. Transmission photomicrographs of: wafer 750-2 (a) in plane polarized light and (b) between crossed polarizers, and wafer 751-1 (c) in plane polarized light and (d) between crossed polarizers, showing the high optical quality and absence of macroscopic strain in these CaF_2-based materials. The field of view is approximately 1 cm^2.

The eventual successful "cure" comprised two changes in procedure:

(1) The total crystal growth and annealing time, typically about 40 hours during the period of the "epidemic," was shortened to 21 to 24 hours. Shorter annealing times than this frequently resulted in high crystal strain and cracked boules.

Slower crystal growth and longer annealing times are effective in reducing crystal strain. We have not been able to detect any macroscopic strain, however, in wafers cut from the more rapidly cooled crystals.

Slower crystal growth, on the other hand, also allows for the escape of the high-vapor-pressure Na dopant, which was initially included for the purpose of inhibiting "blotch" formation. In addition, longer annealing times allow, at the appropriate temperatures, for motion and clustering of the La or Ce impurities. It is some such clustering that is believed to be responsible for the non-photochromic "blotch" absorption.

(2) The standard one-hour duration of the AC treatment was reduced to one-half hour. This has resulted in somewhat higher optimum Ca-vapor pressures for the treatment of most crystals. Again, the shorter time at the elevated AC temperatures probably reduces impurity migration and clustering.

An indication of the success of the above "cure" is the fact that the photochromic absorption changes exhibited by the latest wafers, prepared as indicated, are comparable to, or slightly greater than, those of the best CaF_2 materials we have previously tested. These are the wafers listed in Table I and evaluated in this Report.

B. $SrTiO_3$

1. CRYSTALS

All of the $SrTiO_3$:Ni,Mo,Al photochromic wafers used in this study came from the same single crystal. That crystal was grown by a flame-fusion technique by L. Merker of the Titanium Division of the National Lead Company. Essentially all of the photochromic crystals of transition-metal-doped $SrTiO_3$ studied at RCA Laboratories over the past several years have been supplied by the National Lead Company. As with the CaF_2 systems, however, the photochromic properties of these crystals still vary considerably, even among nominally identical boules.

The optical quality of these $SrTiO_3$ crystals is generally not quite as good as that of CaF_2 but varies from crystal to crystal. As might be expected, the optical quality is generally best in relatively small $SrTiO_3$ boules with low dopant concentrations. These conditions are somewhat incompatible with those for useful photochromic wafers. The optical quality of the crystal used in the present study is illustrated by the transmission photomicrographs of wafer ST-2-0 shown in Figure 2. Figures 2(a) and 2(b) show, respectively, direct transmission and transmission with the wafer between crossed polaroids. Figure 2(b) shows signs of appreciable strain. The maximum dimensions of this wafer are approximately 2.2 by 2.8 cm.

Wafer ST-2-0

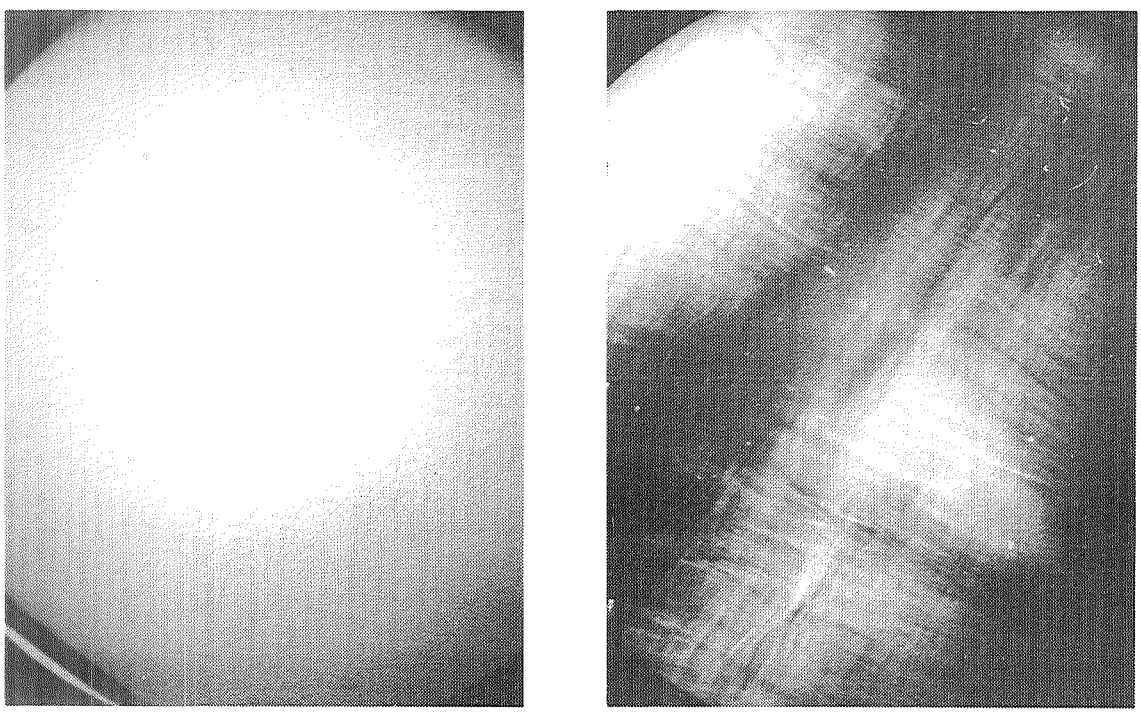

(a) (b)

Figure 2. Transmission photomicrographs of wafer ST-2-0 (a) in plane polarized light and (b) between crossed polarizers, showing signs of macroscopic strain. The field of view is approximately 1 cm^2.

The state-of-the-art is such that the largest area single-crystal photochromic wafers available are those of $SrTiO_3$. Several wafers of $SrTiO_3$:Ni,Mo,Al which were delivered to NASA at the completion of an earlier phase of the present contract[5] had areas of about 6 cm^2 each, even after being trimmed to approximately a 4:3 rectangular aspect ratio. Those wafers, however, exhibited an appreciable striated non-uniformity in color, probably resulting from bulk variations in dopant concentration. The crystal under study in the present case was somewhat smaller but considerably more uniformily colored. (See discussion below). It was cut into wafers of the desired thicknesses and of the largest areas possible. As with the CaF_2, because of the shape of the boule only a few wafers actually came very close to the maximum area, about 5 cm^2. Each wafer was given a high optical polish on both surfaces.

2. HEAT TREATMENT

As-grown $SrTiO_3$:Ni,Mo,Al crystals are already photochromic. But improved photochromic performance and a lower background absorption can be obtained by appropriate heat treatment of the sample wafers. These heat treatments cause changes in the valence states of the Ni and Mo impurity ions, probably by varying the concentration of oxygen vacancies in the $SrTiO_3$ crystal. Both oxidation and reduction treatments can be carried out reversibly and have been studied and described by Faughnan and Kiss[3,6]. As is generally the case, the wafers under consideration here required a mild reduction treatment for maximum unswitched transmission.

3. EFFORTS TOWARD IMPROVEMENT

As discussed above, large area wafers of photochromic $SrTiO_3$:Ni,Mo,Al have been tested and delivered to NASA under earlier phases of the present contract. In ordering another crystal boule of this material for evaluation in the current phase, we sought three improvements:

(1) A larger boule, one capable of providing trimmed wafers about 3.0 x 2.3 cm, or 7 cm^2 in area;

(2) Higher dopant concentrations for larger photochromic absorption changes; and

(3) Greater uniformity in dopant concentration throughout the crystal.

These improvements have turned out to be incompatible with the present state-of-the-art. The crystal supplied by the National Lead Company

and used in this study does contain a dopant concentration approximately 2.5 times that of the earlier boule[5]. The higher concentration, however, did not result in greater photochromic absorption changes as had been hoped. In that respect the new material is about comparable to that reported on previously. On the other hand, the uniformity of dopant concentration and coloration is greatly improved. No non-uniformity at all is readily visible to the unaided eye. This is particularly impressive in view of the higher dopant concentration present. Finally, the size of the crystal boule is such that the maximum wafer area obtained is about 5 cm^2 untrimmed, somewhat smaller than those supplied to NSSA earlier. In addition, as shown in Figure 2, even this boule size was not achieved without some crystal strain.

C. $CaTiO_3$

1. CRYSTALS

Wafers from four different $CaTiO_3$:Ni,Mo crystal boules have been used in the present study. These crystals, like that of $SrTiO_3$, have been supplied by the National Lead Company. The crystals were grown by a flame-fusion technique developed there by L. Merker[7]. Using a high-temperature annealing procedure, Merker was able to prevent, in large pure $CaTiO_3$ single crystals, the severe twinning and cracking common to both natural and synthetic crystals, regardless of size. With the addition of dopants such as Ni and Mo to make the $CaTiO_3$ photochromic, the twinning and cracking reappeared. It has been necessary, therefore, to modify the crystal growth and annealing procedures.

Extensive efforts by the National Lead Company to improve the crystal quality of doped $CaTiO_3$ met with some success at first. Significant progress toward increasing the crack-free and twin-free volumes of such crystals were illustrated and discussed in the last progress report[1]. Unfortunately that progress has not continued. In spite of continued effort, in fact, it has not even been possible to reproduce those earlier improvements.

The last two $CaTiO_3$:Ni,Mo wafers listed in Table I are from those crystal boules which did exhibit improved optical quality. The other four wafers were cut from more recently grown boules. Transmission photomicrographs of one wafer from each crystal boule used in this study are shown in Figure 3.. Actual cracks show up clearly in the direct transmission pictures of Figures 3(a),(c),(e), and (g). The lamellar twinning structure becomes clearer when the wafers are placed between crossed polarizers as in Figures 3(b),(d),(f), and (h).

Wafer CT-3A

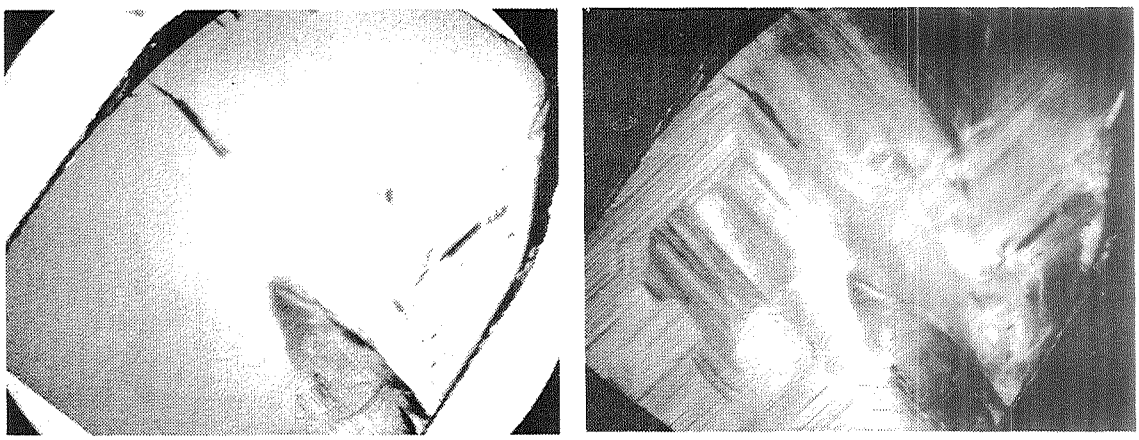

(a) (b)

Wafer CT-1-1

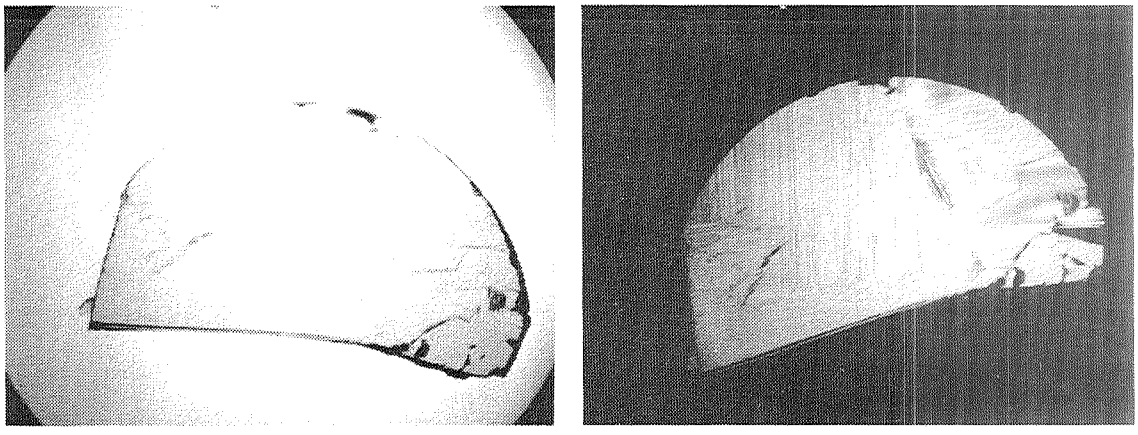

(c) (d)

Figure 3. Transmission photomicrographs of wafers cut from four different crystal boules of $CaTiO_3$:Ni,Mo. Direct transmission pictures show moderate cracking in recent boules, (a) and (c), but less extensive cracking in earlier improved boules, (e) and (g). Placed between crossed polarizers, all wafers exhibited extensive lamellar twinning, (b), (d), (f), and (h). The field of view is approximately 1 cm^2.

Wafer CT-1-0

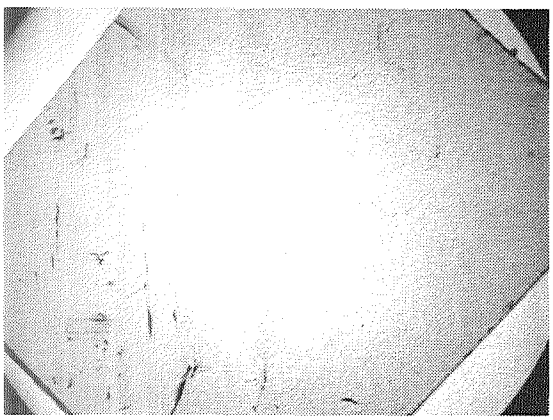

(e)

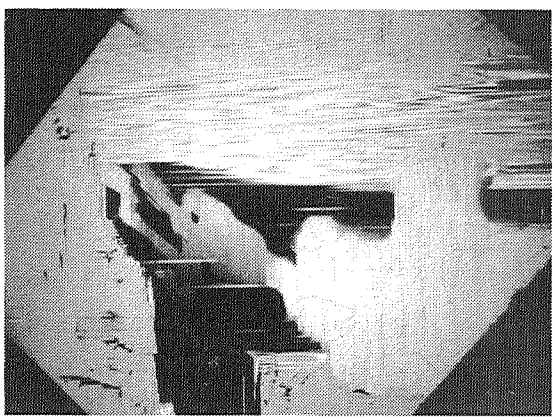

(f)

Wafer CT-2C-0

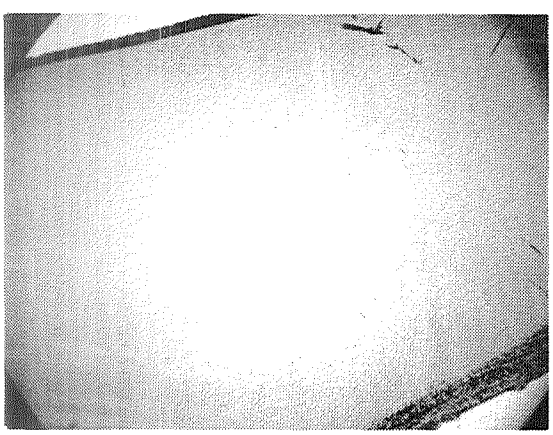

(g)

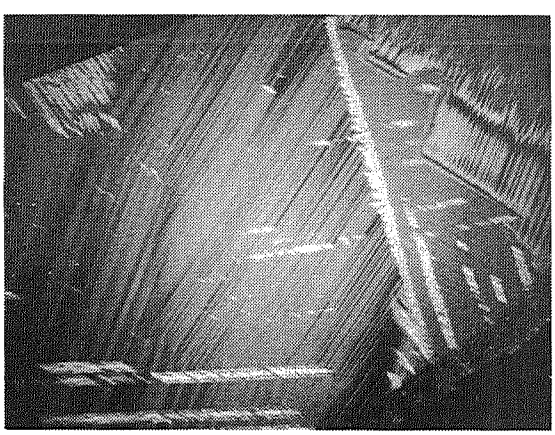

(h)

Figure 3. (Continued).

Because of the cracking problem $CaTiO_3$ crystal boules are usually relatively small. In addition, the crystals are somewhat more fragile than those of $SrTiO_3$ and more subject to breakage during cutting, polishing, and handling. Nevertheless, a number of wafers of reasonable size were successfully cut, optically polished on both surfaces, and tested. The largest of these, CT-2C-O, came from one of the boules of high optical quality and has dimensions of about 1 by 2 cm.

2. HEAT TREATMENT.

The as-grown $CaTiO_3$:Ni,Mo crystals have a deep reddish-brown, or wine, color. A mild reducing heat treatment of the finished wafers, similar to that used for the $SrTiO_3$:Ni,Mo,Al wafers, was sufficient to significantly reduce this background absorption, in some cases to almost completely eliminate it. The photochromic absorption changes attainable also appeared to be somewhat increased by this treatment.

III. PHOTOCHROMIC ABSORPTION SPECTRA

A. EXPERIMENTAL PROCEDURES AND RESULTS

The photochromic absorption spectra of 15 of the 17 sample wafers listed in Table I are shown in Appendix A, Figures A-1 through A-15. The order is the same as that in Table I. In all cases, the absorption spectra of the unswitched or thermally stable states are indicated by the solid curves, those of the switched states by the broken curves. Where the spectra of the optically erased states differ from those of the unswitched states, they are indicated by long-short dashed curves.

The absorption spectra were recorded on a Cary-14 spectrophotometer. Because of the relatively short thermal lifetimes of their photochromic switched states, wafers of $SrTiO_3$:Ni,Mo,Al and $CaTiO_3$:Ni,Mo were re-switched several times during the recording of their switched-state spectra. These spectra, the broken curves in Figure A-8 through A-15, have thus been corrected for the thermal decay which occurred during recording.

The absorption spectra of the thermally stable states were recorded after the wafers had been heated to about 150°C for about two minutes and cooled to room temperature in the dark. Subsequently, the wafers were switched and optically erased with suitably filtered and focused radiation from an Osram HBO-500W 500 W Hg lamp. The filters used for switching purposes were approximately one centimeter of saturated $CuSO_4$ solution and either a Corning 7-59, 0-51 filter combination (for CaF_2), or a Corning 7-54 filter (for $SrTiO_3$ and $CaTiO_3$). All optical erasing was done through about one centimeter of H_2O and a Corning 3-71 filter. The standard switching exposure was two minutes, and each wafer was exposed from one side only. The standard erasing exposure was one minute for $SrTiO_3$ and $CaTiO_3$, three minutes for CaF_2.

The general features of these absorption spectra are well known by now and will not be discussed here. For comparison and evaluation purposes, the most important quantitative data that can be extracted from these spectra are the maximum photochromic changes in absorption, Δ OD, at wavelengths of special interest. Such data, for each host-dopant combination, are summarized in Tables II through V. Using these values of Δ OD and the wafer thicknesses, changes in the average bulk absorption coefficient have been calculated for each case and are also recorded, as $\Delta\alpha$, in these tables.

The wavelengths for which these data are tabulated include those corresponding to maximum photochromic absorption changes for each respective material. Also included is the argon laser output wavelength, 5145 Å, which lies closest to the visible readout and erase bands of these materials. An argon laser operating at 5145 Å would appear to be an excellent

T A B L E II

CaF_2:La,Na PHOTOCHROMIC SPECTRA SUMMARY

Wafer No.	Thickness (mm)	Saturated Absorption Changes					
		λ = 5145 Å		λ = 5750 Å		λ = 4130 Å	
		Δ OD	$\Delta\alpha$ (cm^{-1})	Δ OD	$\Delta\alpha$ (cm^{-1})	Δ OD	$\Delta\alpha$ (cm^{-1})
750-2	0.81	0.33	9.0	0.43	12	- 0.82	- 23
750-3	0.53	0.23	11.	0.28	12	- 0.52	- 23
750-4	0.29	0.12	9.4	0.16	12	- 0.27	- 21
750-5	0.13	0.06	11.	0.075	14	- 0.14	- 25

source for coherent optical processing and could also be used for recording on these materials in the erase mode. For these reasons, this argon laser line has been used to measure the erase mode sensitivity of these wafers (see Section IV). The data summarized in Tables II through V are discussed briefly below.

B. DISCUSSION

1. CaF_2:La,Na

The photochromic absorption spectra of the four CaF_2:La,Na wafers are shown in Figures A-1 through A-4 of Appendix A and summarized in Table II. The lack of any dependence of $\Delta\alpha$ on wafer thickness in Table II indicates that, at least at saturation switching, photochromic coloration is indeed a bulk phenomenon in CaF_2:La,Na. This is probably less true for less than saturated switching, however.

Clearly the most sensitive readout wavelength for these wafers is 4130 Å. (The negative values of Δ OD and $\Delta\alpha$ here indicate that absorption at this wavelength decreases as these wafers are switched). The readout sensitivity at the argon 5145 Å line is less by about a factor of two. It is also clear that for 5145 Å readout, a transmission contrast ratio of 2:1 (Δ OD = 0.30) could only be provided by the thickest wafer tested.

Greater photochromic absorption changes, by a factor of 1.5 or more, can be induced in these CaF_2:La,Na wafers (and, to a lesser extent, in the CaF_2:Ce,Na wafers as well) if the 7-59, 0-51 Corning filter combination used to limit the switching radiation is replaced by a Corning 7-54 filter only. The greater switching results primarily from the increased intensity of Hg 3650 Å radiation in the switching light. However, not all of this increased photochromic absorption change can be optically erased. In fact, the optically reversible portion of this change is essentially the same as that shown in Figures A-1 through A-4. It was for this reason that the more conservative 7-59, 0-51 Corning filter combination was used here. As the long-short dashed curves in these figures indicate, optical erasure is not absolutely complete even under these conditions.

2. CaF_2:Ce,Na

The photochromic absorption spectra of the three CaF_2:Ce,Na wafers are shown in Figures A-5 through A-7 of Appendix A and summarized in Table III. Since the argon 5145 Å line lies so close to the peak of the visible switched-state absorption band of photochromic CaF_2:Ce,Na, data for only one of these wavelengths, that of the laser line, are included in Table III. The 4000 Å band here corresponds to the 4130 Å band of CaF_2:La,Na discussed above. The third wavelength for which data is included in Table III is 7000 Å, the peak of the "non-destructive" readout band of CaF_2:Ce,Na. While, as has been pointed out in previous reports[1], this band is indeed relatively "non-destructive," it is for present purposes hardly deserving of the name "readout band" because of its extremely

T A B L E III

CaF_2:Ce,Na PHOTOCHROMIC SPECTRA SUMMARY

Wafer No.	Thickness (mm)	Saturated Absorption Changes					
		λ = 5145 Å		λ = 4000 Å		λ = 7000 Å	
		Δ OD	Δα (cm^{-1})	Δ OD	Δα (cm^{-1})	Δ OD	Δα (cm^{-1})
751-1	0.86	0.27	7.2	-0.59	-16	-0.09	-2
751-2	0.53	0.18	7.8	-0.38	-16	-0.06	-3
751-3	0.32	0.10	7.3	-0.21	-15	-0.04	-3

poor sensitivity to photochromic absorption changes as shown by the very small values of Δ OD recorded in Table III.

Otherwise, all of the observations made in sub-section A above concerning the data in Table II on the CaF_2:La,Na wafers are equally applicable here.

3. $SrTiO_3$:Ni,Mo,Al

From Figures A-8 through A-11 of Appendix A it is apparent that the argon laser line at 5145 Å falls very near the peak of the switched-state absorption band of photochromic $SrTiO_3$:Ni,Mo,Al. Therefore, data for only one of these wavelengths, that of the laser, are given in Table IV.

The data for photochromic $SrTiO_3$:Ni,Mo,Al shown in Table IV differs in two distinct ways from that for photochromic CaF_2 recorded in Tables II and III. First, the absolute saturated photochromic absorption changes are markedly greater for $SrTiO_3$:Ni,Mo,Al. Even the thinnest wafer tested is capable of producing a transmission contrast ratio of nearly 3:1 at the 5145 Å readout wavelength.

Second, the quantity Δα at this same readout wavelength shows a marked dependence on wafer thickness. This dependence has been discussed in previous reports[5]. It results from the fact that photochromic coloration is not truly a bulk phenomenon in $SrTiO_3$:Ni,Mo,Al[3]. The very limited

T A B L E IV

$SrTiO_3$:Ni,Mo,Al PHOTOCHROMIC SPECTRA SUMMARY

Wafer No.	Thickness (mm)	Saturated Absorption Change	
		λ = 5145 Å	
		Δ OD	Δα (cm^{-1})
ST-2-0	1.02	0.86	20
St-2-4	0.53	0.73	32
St-2-6	0.28	0.60	50
St-2-10	0.18	0.45	58

penetration depth of the strongly absorbed switching radiation confines photochromic coloration to a relatively thin surface layer, which then becomes the effective photochromic thickness of the wafer.

4. $CaTiO_3$:Ni,Mo

The photochromic spectra of $CaTiO_3$:Ni,Mo, shown in Figures A-12 through A-15 of Appendix A and summarized in Table V, are very similar in many ways to those of $SrTiO_3$:Ni,Mo,Al. The absolute photochromic absorption changes at the 5145 Å readout wavelength are somewhat larger, making possible a transmission contrast ratio of greater than 3.5:1 (Δ OD = 0.545) with the thinnest wafer tested.

The quantity $\Delta\alpha$ appears, in Table V, to be relatively independent of wafer thickness. This is somewhat deceiving. It is primarily a result of the lack of reproducibility of the photochromic properties of state-of-the-art $CaTiO_3$:Ni,Mo. The four wafers studied represent two different crystal boules and rather widely separated regions of one of them. In fact, while the depth of photochromic coloration is perhaps somewhat greater in $CaTiO_3$:Ni,Mo than in $SrTiO_3$:Ni,Mo,Al under the conditions of these experiments, it remains a surface phenomenon to a large extent.

T A B L E V

$CaTiO_3$:Ni,Mo PHOTOCHROMIC SPECTRA SUMMARY

Wafer No.	Thickness (mm)	Saturated Absorption Change	
		λ = 5145 Å	
		Δ OD	$\Delta\alpha$ (cm^{-1})
CT-3A	0.81	2.20	63
CT-1-1	0.56	1.44	60
CT-3C-2	0.31	0.80	61
CT-3C-1	0.18	0.55	72

IV. ERASE MODE SENSITIVITY

A. THE ERASE MODE

Wafers of the photochromic materials under study here are of interest as information input planes for coherent optical processing systems. How is the information to be recorded on them? In many ways, the most attractive proposal is to use a modulated, scanned, and focused laser bean to "write" the desired information onto such a wafer, *in situ*, in the optical processor. Unfortunately, however, there are no lasers in existence which operate at an appropriate wavelength with sufficient power to permit efficient and high speed recording on any of these materials in the usual "write," or switching, mode.

On the other hand, the argon laser is capable of output powers of several watts at wavelengths near 5000 Å. In particular, the argon 5145 Å line is remarkably well matched to the peaks of the visible readout and erase bands of all four of these materials. It is interesting, therefore, to consider the possibility of using a 5145 Å argon laser, appropriately modulated and scanned, to record in the erase mode on wafers which have been uniformly pre-switched with appropriate near-UV radiation. The switching light, of course, need not be coherent. This scheme also offers the possible advantage of using the same wavelength of light, perhaps even a single laser source, for both recording and readout.

In several previous studies[1,3,8,9], some of them carried out during earlier phases of this contract, considerable attention has been focused on the quantum efficiencies and sensitivities of various inorganic photochromic materials used in the write mode. Some, but considerably less, attention has been paid to the sensitivities of some of these same materials operated in the erase mode[8].

In this Section, therefore, we describe and discuss detailed erase mode sensitometric measurements at 5145 Å, made on each of the first 15 wafer samples listed in Table I, those for which photochromic absorption spectra have been obtained (Appendix A).

B. EXPERIMENTAL PROCEDURE

Each photochromic wafer tested was first switched to saturation using appropriately filtered radiation from an Hg lamp, as described in Section III. A. The wafer was then (within two seconds) placed in and perpendicular to the output beam of an argon laser operating at 5145 Å. The intensity of this erase beam transmitted through the wafer was monitored by a linear detector (PIN diode) and displayed as a function of time on either an oscilloscope or an x-y recorder, depending on how fast

or slowly the erasure proceeded. Thus, readout and erasure were accomplished with the single source and a single beam.

The maximum power output of the laser in this single line was approximately one watt. With control of the beam diameter (using a beam expander) and the laser tube plasma current, and with the addition of beam attenuators, we were able to vary the erase beam intensity at a 1/16 inch sample aperture by more than four orders of magnitude, from about 2 W/cm^2 down to less than 0.2 mW/cm^2. The absolute beam intensity was measured directly with a recently calibrated Eppley thermopile. For each wafer, the transmission-versus-time-of-exposure characteristic was recorded at several different levels of erase beam power.

For most of the wafers studied, room temperature thermal decay characteristics were also determined. Such data were taken using the lowest detectable readout (and erase) beam intensity and blocking the wafer from exposure to even that beam except for brief periodic measurements.

C. SENSITIVITY CURVES

The resulting families of erase mode sensitivity curves are shown in Figures B-1 through B-15 in Appendix B. The order of the figures is the same as that of the first 15 wafer samples listed in Table I and the same as that of the photochromic absorption spectra in Appendix A. The display format used, optical density change versus logarithm of exposure, emphasizes. the middle exposure range where most of the optical density change occurs and is the standard format used for sensitometric data on photographic film.

In a general way, these families of sensitivity curves behave as expected:

1. Clearly the CaF_2-based photochromic materials have the slowest room temperature thermal decay, the optical density dropping by about 30% in 1000 sec for CaF_2:La,Na (Figures B-1 through B-4) and about 15% in 1000 sec for CaF_2:Ce,Na (Figures B-5 through B-7). The $SrTiO_3$:Ni,Mo,Al wafers (Figures B-8 through B-11), on the other hand, have the most rapid thermal decay, the optical density falling by a factor of two in 15 to 40 seconds. The corresponding decay times for the $CaTiO_3$:Ni,Mo wafers appear to be 15 to 50 minutes, almost two orders of magnitude longer.
2. When the optical erase beam is added, in each case, the optical density falls away from the thermal decay curve and decreases more rapidly. As the erase beam intensity is increased, this occurs at earlier and earlier times, and the erase curve approaches a fixed shape with a central region of fixed slope or γ.

D. SENSITOMETRIC CHARACTERISTICS

If time-intensity reciprocity holds for the erase mode operation of these photochromic wafers, then the entire family of sensitivity curves for each wafer should coalesce into a single sensitometric characteristic when the same optical density changes are replotted as a function of erase exposure energy density (i.e. the product of erase beam intensity and exposure time) rather than of exposure time alone. Such erase mode sensitometric characteristics are shown in Figures 4 through 7 for one wafer of each of the four materials studied.

1. CaF_2:La,Na AND CaF_2:Ce,Na

The sensitivity curves for wafers 750-3 and 751-2 are shown in Figures B-2 and B-6 (Appendix B) respectively. The solid points in Figures 4 and 5 respectively represent sensitometric data for these two wafers, calculated from those curves in the manner described above. As indicated, they

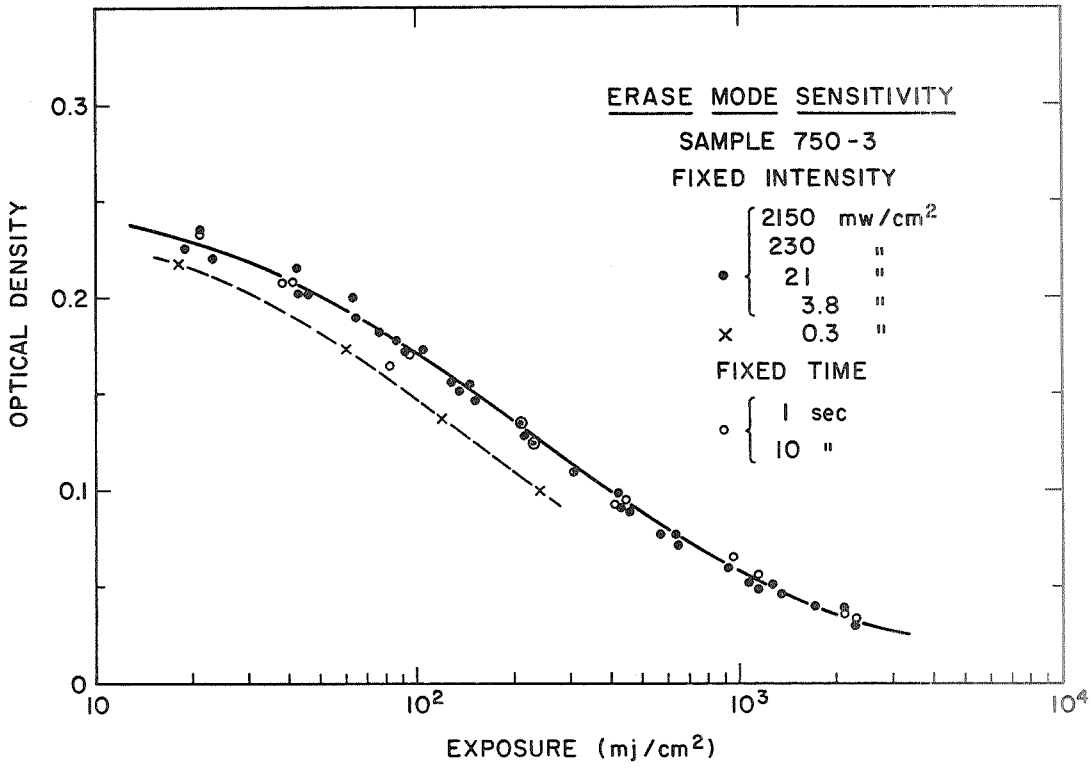

Figure 4. Erase Mode Sensitometric Characteristic for CaF_2:La,Na wafer 750-3, showing a high degree of time-intensity reciprocity.

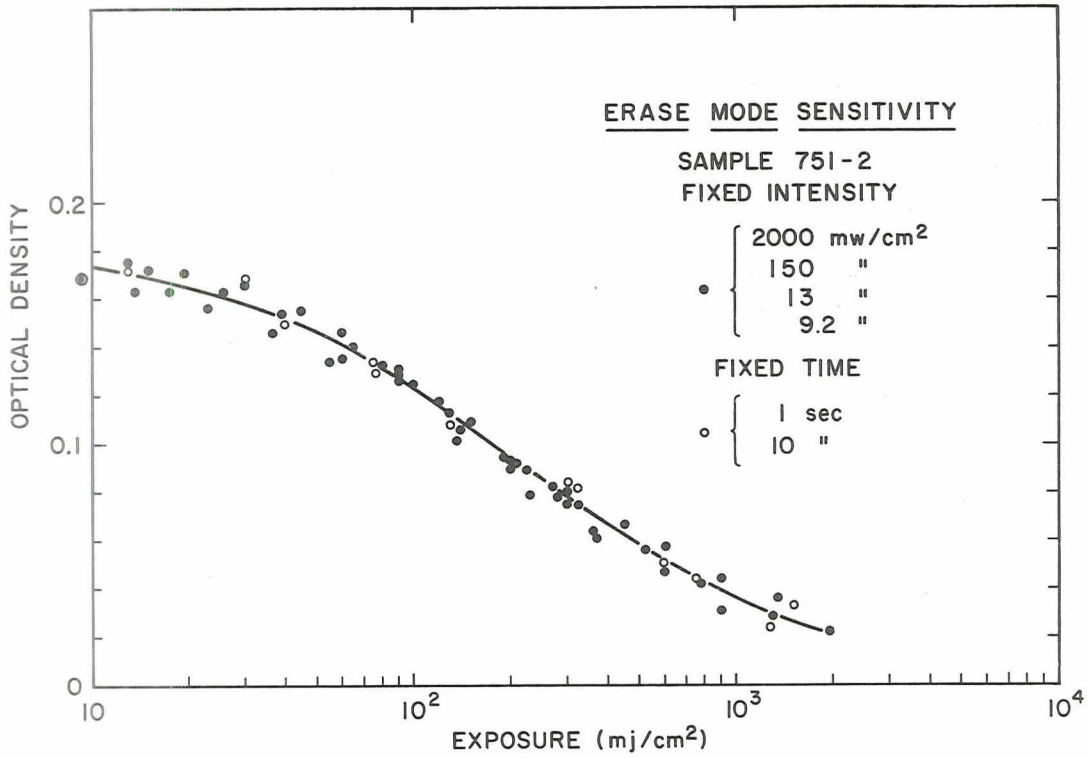

Figure 5. Erase Mode Sensitometric Characteristic for CaF_2:Ce,Na wafer 751-2, showing a high degree of time-intensity reciprocity.

correspond to four erase beam intensities spanning nearby three orders of magnitude. In each case, the four separate curves have indeed coalesced to such a degree that they are now well represented by single sensitometric characteristics.

These same characteristic curves can, of course, also be determined in another way, as is demonstrated by the open circle points in Figures 4 and 5. These points correspond to the erasures achieved in two fixed times, as indicated, by various erase beam intensities, again using data from Figures B-2 and B-6.

The x-points in Figure 4 were determined in the same manner as were the solid points, but for an erase intensity smaller by another factor of ten, as shown. It appears that time-intensity reciprocity is beginning to fail at such low beam intensities. This can be related, both qualitatively and semiquantitatively, to the thermal decay that takes place on about the same time scale, as can be seen in Figures B-1 through B-4.

2. $SrTiO_3$:Ni,Mo,Al AND $CaTiO_3$:Ni,Mo

The sensitivity curves for wafers ST-2-10 and CT-1-1 are shown in Figures B-11 and B-13 (Appendix B) respectively. The solid curves in Figures 6 and 7 represent sensitometric data, for these two wafers respectively, calculated from those sensitivity curves in the manner described earlier (and used above to determine the solid points in Figures 4 and 5). They correspond to different erase beam intensities spanning over three decades (over four decades in Figure 7). Unlike the similar curves in Figures 4 and 5 for the CaF_2-based materials, these curves have not coalesced to single sensitometric characteristics for each wafer.

The broken curves in Figures 6 and 7 show the erasures achieved in two or three fixed times, as indicated, by various erase beam intensities, again using the sensitivity curves of Figures B-11 and B-13.

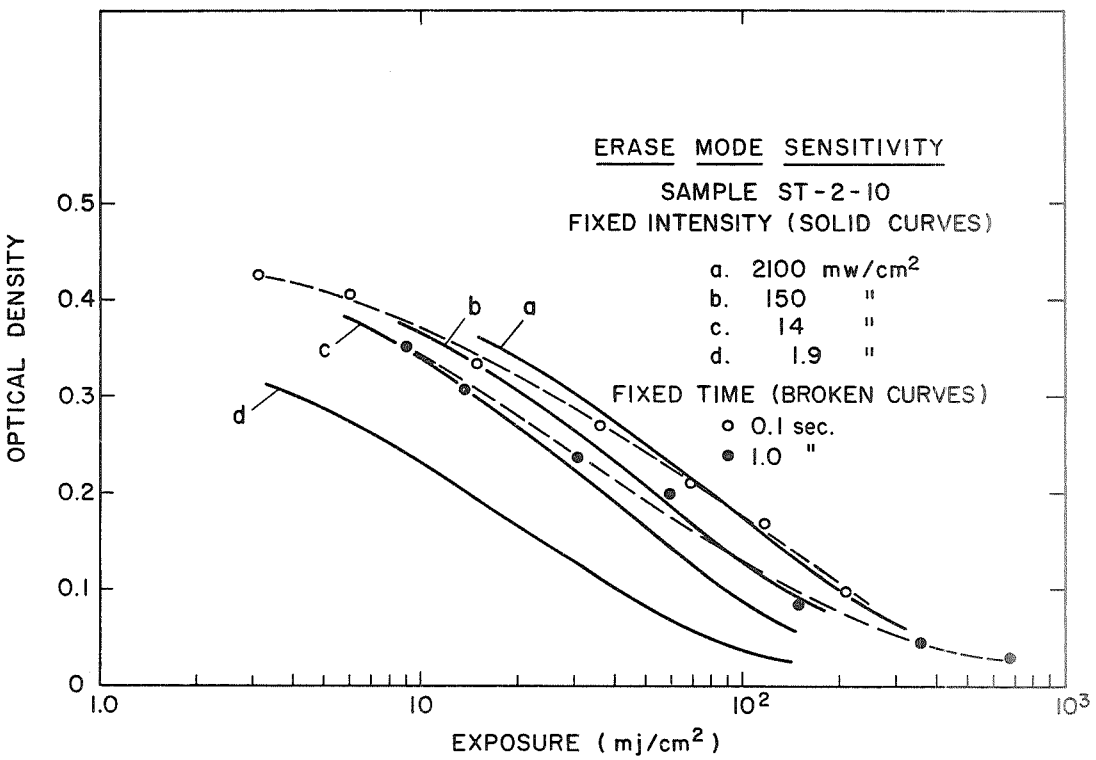

Figure 6. Erase Mode Sensitometric Characteristics for $SrTiO_3$:Ni,Mo,Al wafer ST-2-10, showing failure of time-intensity reciprocity.

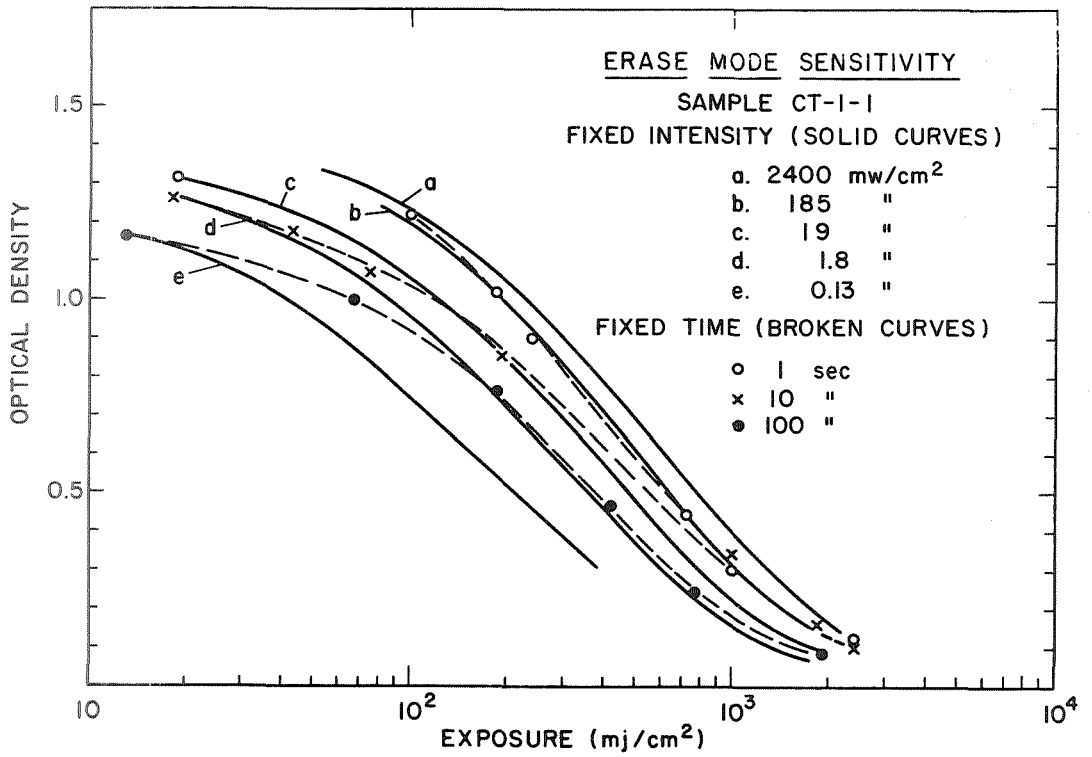

Figure 7. Erase Mode Sensitometric Characteristics for $CaTiO_3$:Ni,Mo wafer CT-1-1, showing failure of time-intensity reciprocity.

Clearly, time-intensity reciprocity does not hold for the erase mode operation of these titinate-based wafers, even at the highest erase beam intensities used. Thus, no single sensitometric characteristics exist for the intensity range studied. These materials exhibit a much more rapid thermal decay than do the CaF_2-based photochromics, and the more severe reciprocity failure is qualitatively, and probably to some extent quantitatively, related thereto.

E. TIME-INTENSITY RECIPROCITY

Erase mode time-intensity reciprocity is investigated directly in Figures 8 through 11. The time-of-erasure is plotted against the erase beam intensity for each of the first 15 sample wafers listed in Table I. The data plotted for each wafer were taken directly from the corresponding

families of sensitivity curves shown in Figures B-1 through B-15 (Appendix B). In most cases the range of erase intensities spans nearly four decades, in some cases more than four. The time-of-erasure used is $T_{1/2}$, the time required for the readout optical density to be reduced to half its initial value.

I. CaF_2:La,Na AND CaF_2:Ce,Na

Figures 8 and 9 show these "reciprocity characteristics" for the four CaF_2:La,Na wafers and the three CaF_2:Ce,Na wafers respectively. For erase beam intensities greater than about 10mW/cm^2, all seven wafers exhibit almost the perfect inverse relationship required for true reciprocity. Reciprocity begins to fail very gradually for smaller intensities, or for values of $T_{1/2} \lesssim$ 10 to 40 sec. This failure occurs first (i.e. at the highest intensity) for wafer 750-5, the thinnest of the seven samples.

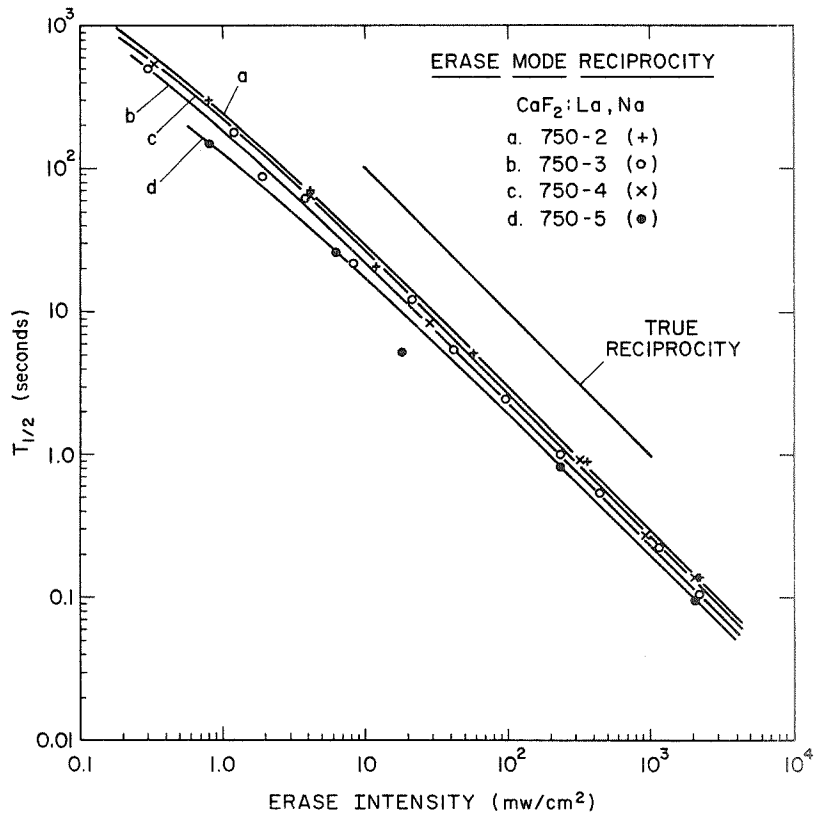

Figure 8. Erase Time $T_{1/2}$ (to half-OD point) versus Erase Beam Intensity for four wafers of CaF_2:La,Na.

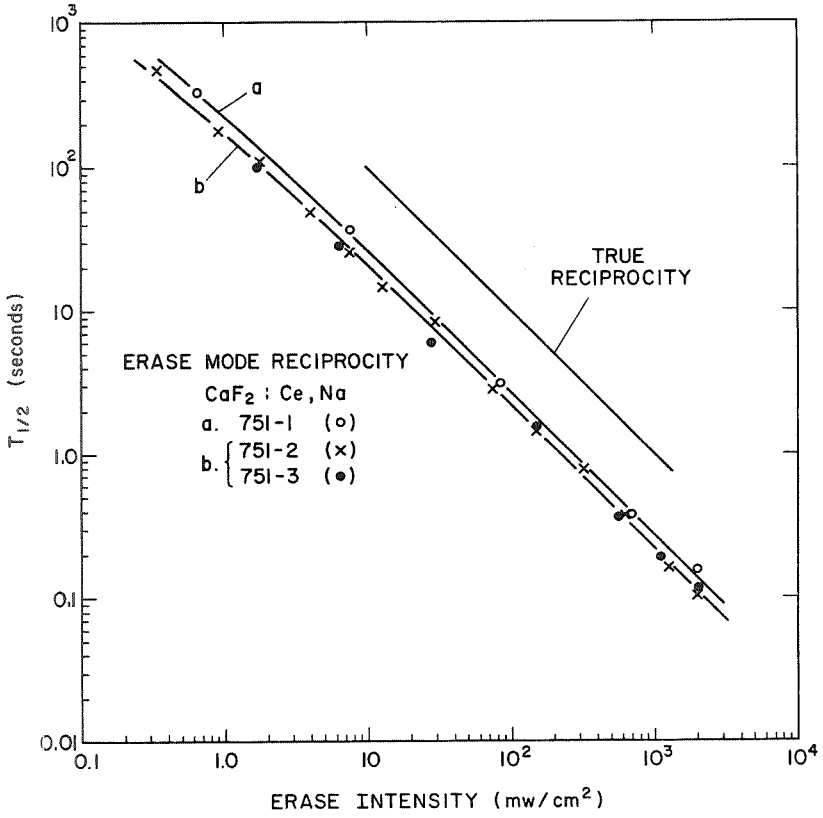

Figure 9. Erase Time $T_{1/2}$ (to half-OD point) versus Erase Beam Intensity for three wafers of CaF_2:Ce,Na.

The reported values of $T_{1/2}$ corresponding to thermal decay alone are $T_{1/2}$ (thermal) $\approx 7 \times 10^4$sec. and $\approx 6 \times 10^5$sec. for CaF_2:La and CaF_2Ce (both without Na) respectively[10]. Thus, reciprocity begins to fail at values of $T_{1/2}/T_{1/2}$ (thermal) $\lesssim 10^{-3}$ to 10^{-4}.

These results confirm, and generalize to other wafers, the reciprocity observed for wafers 750-3 and 751-2 in Figures 4 and 5.

2. $SrTiO_3$:Ni,Mo,Al AND $CaTiO_3$:Ni,Mo

Figures 10 and 11 show the "reciprocity characteristics" for the four $SrTiO_3$:Ni,Mo,Al wafers and the four $CaTiO_3$:Ni,Mo wafers respectively. Even at the highest intensities used, none of these wafers show true time-intensity reciprocity. Instead, $T_{1/2}$ varies as about the inverse 0.9 power

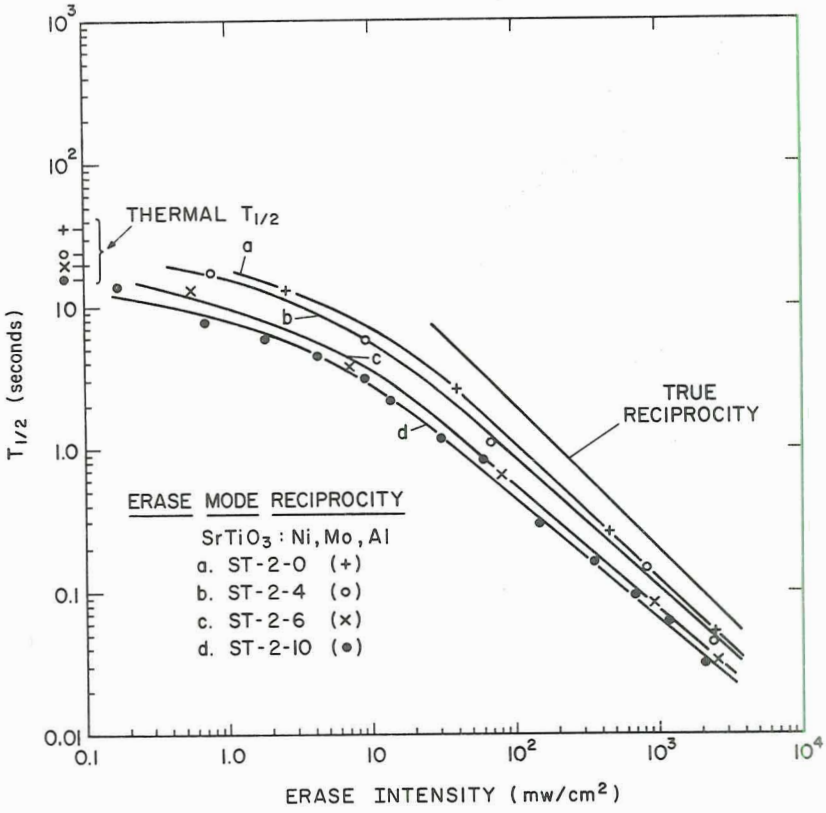

Figure 10. Erase Time $T_{1/2}$ (to half OD point) versus Erase Beam Intensity for four wafers of $CaTiO_3$:Ni,Mo.

of the erase intensity in this range. This is not necessarily inconsistent with the above results for the CaF_2 materials, however. There, the criterion for true reciprocity appeared to be $T_{1/2}/T_{1/2}$ (thermal) $\gtrsim 10^{-3}$ to 10^{-4}. For $SrTiO_3$:Ni,Mo,Al and $CaTiO_3$:Ni,Mo the values of $T_{1/2}$ (thermal), about 25 $\pm$ 10 sec. and about 10^3 sec. respectively, are much smaller. Thus, even at the highest powers used, the criterion above is, at best, barely satisfied.

For the $SrTiO_3$ wafers reciprocity fails very badly at erase intensities smaller than about 40 mW/cm^2 or values of $T_{1/2} \gtrsim 1.5$ sec. For the $CaTiO_3$ wafers, on the other hand, the inverse 0.9 power dependence of $T_{1/2}$ on erase intensity continues to somewhat below 10 mW/cm^2 and values of $T_{1/2} \approx 20 \pm 10$ sec.

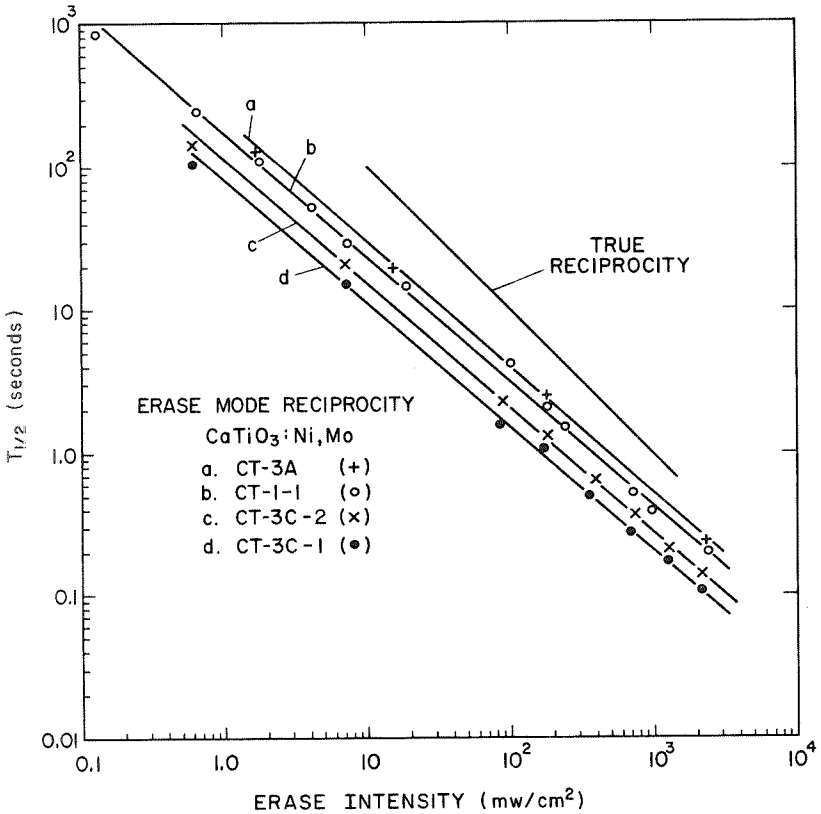

Figure 11. Erase Time $T_{1/2}$ (to half OD point) versus Erase Beam Intensity for four wafers of $CaTiO_3$:Ni,Mo.

F. SUMMARY

Some of the quantitative sensitometric data obtained in these experiments and discussed in this Section of this Final Report are very briefly summarized and compared in Tables VI and VII, for the CaF_2-based wafers and the titinate-based wafers respectively. The wafer numbers correspond to those introduced in Table I. Maximum photochromic optical density changes, OD_{max}, at 5145 Å were obtained from the sensitivity curves of Figures B-1 through B-15 (Appendix B). The quantity γ is defined as the slope of the nearly linear central region of a given one of these sensitivity curves. The quantity $\bar{\gamma}$ is the average value of γ for the family of sensitivity curves for a given wafer. The time, $T_{1/2}$, required for erasure of a given wafer to half its initial optical density, can be obtained from Figures 8 through 11 for any of a wide range of erase beam intensities. The product of $T_{1/2}$ and the corresponding beam intensity then gives the exposure, $E_{1/2}$, required to reduce the optical density to half its initial value.

T A B L E VI

CaF_2 ERASE MODE SENSITOMETRY SUMMARY

Wafer No.	OD_{max} at 5145 Å	γ*		$T_{1/2}$(sec.) (at 1W/cm^2)	$E_{1/2}$(mJ/cm^2) (at 1W/cm^2)
		$\bar{\gamma}$	$\bar{\gamma}/OD_{max}$		
750-2	0.36	0.034	0.45 ± .03	0.29	290
750-3	0.25	0.058	0.45 ± .03	0.23	230
750-4	0.13	0.12	0.48 ± 0.2	0.27	270
750-5	0.076	0.18	0.50 ± .04	0.19	190
751-1	0.27	0.14	0.51 ± .03	0.27	270
751-2	0.18	0.095	0.51 ± .04	0.22	220
751-3	0.10	0.057	0.57 ± .06	0.22	220

*For erase beam intensities > 1mW/cm^2.

T A B L E VII

$SrTiO_3$ AND $CaTiO_3$ ERASE MODE SENSITOMETRY SUMMARY

Wafer No.	OD_{max} at 5145 Å	γ*		$T_{1/2}$(sec.) (at 1W/cm^2)	$E_{1/2}$(mJ/cm^2) (at 1W/cm^2)
		$\bar{\gamma}$	$\bar{\gamma}/OD_{max}$		
ST-2-0	0.90	0.57	0.63 ± .05	0.12	120
ST-2-4	0.79	0.46	0.58 ± .04	0.11	110
ST-2-6	0.48	0.31	0.65 ± .02	0.077	77
ST-2-10	0.44	0.26	0.59 ± .03	0.065	65
CT-3A	2.06	1.34	0.65 ± .06	0.53	530
CT-1-1	1.43	0.97	0.68 ± .08	0.42	420
CT-3C-2	0.96	0.65	0.67 ± .04	0.27	270
CT-3C-1	0.52	0.33	0.64 ± .02	0.20	200

*For erase beam intensities > 1mW/cm^2.

V. RESOLUTION

A. THE PROBLEM

Wafers of state-of-the-art single-crystal photochromic materials must be about 100 μm or more thick in order to provide photochromic optical density changes as large as 0.3, i.e. a maximum contrast ratio of 2:1. The actual thickness required depends on the material (both host and dopant) and on the wavelengths of the write and readout light used. By comparison, silver halide photographic film is capable of providing optical densities of greater than 5 in an emulsion thickness of only about 5 μm.

This finite wafer thickness imposes some important restrictions on the resolution capabilities of single-crystal photochromic materials. If optical recording onto, and/or readout from, a wafer of thickness t mm is accomplished in an f/m optical system (i.e. a focused light cone with half-angle $\theta_{1/2} = \tan^{-1}\frac{1}{2m}$), the resolution is limited to about $N_{TV} < \frac{2m}{t}$ TV (raster) lines per mm or $N_{pr} < \frac{m}{t}$ line pairs (one black, one white) per mm. Thus, for a 100 μm wafer and f/10 optics, $N_{TV} < 200$ lines/mm or $N_{pr} < 100$ line pairs/mm. For thicker wafers the resolution capabilities clearly decrease with 1/t.

In a coherent optical data-processing system using photochromic wafer data-input planes, laser sources would probably be used for both recording and readout. Then the f-number, m, could be essentially infinite and resolution would be limited by:

(1) The optical homogeniety of the wafer material.
(2) The varying angle at which a scanning laser recording beam passes through the wafer.
(3) Diffraction effects which cause spreading of the recording or readout light within the wafer.

B. THE EXPERIMENT

In order to demonstrate, in a fairly simple and direct way, the resolution capabilities of the photochromic wafers under study here, we have recorded in each of them a series of line gratings with different grating spacings. The grating masters were prepared on high contrast photographic plates. They were recorded in the erase mode by contact printing onto wafers which had been pre-switched in appropriate U.V. light. The erase-recording light was coherent 5145 Å argon laser radiation. With the master grating removed, readout of the recorded gratings was accomplished by means of transmission photomicrographs, using the same 5145 Å argon radiation at reduced intensity.

C. RESULTS AND DISCUSSION

These transmission photomicrographs of the master gratings and the photochromically recorded reproductions are shown in Figures C-1 and C-2 through C-13, respectively, in Appendix C. The four gratings used had 25, 40, 80, and 100 line pairs per mm (ln. pr./mm). The approximate magnification of the pictures shown is 200 times. The wafer numbers correspond to those established in Table I. The order of the figures is the same as that of the wafers listed in Table I, except that not all wafers listed are included in Appendix C.

The quality of the photomicrographs shown is limited by:

(1) Spacial variations in intensity in the multi-mode laser beam.
(2) Diffraction effects, resulting from specks of dust and dirt.
(3) Low contrast, resulting from the small photochromic optical density changes attainable in the relatively thin wafers, especially those of the CaF_2-based materials.
(4) The reproduction process.

In order to provide as much clarity as possible, one set of the original photomicrographs reproduced in Appendix C is being forwarded to NASA with this Final Report.

In spite of the above limitations, however, we have successfully accomplished both recording and readout of the 100 ln. pr./mm grating in at least one wafer of each material. The most serious problem encountered has been that of low contrast in the thinnest wafers, rather than limited resolution in the thickest wafers. The wafers of each material, however, presented their own difficulties.

1. CaF_2 (FIGURES C-2 THROUGH C-6)

For these wafers the major problem is the limited photochromic optical density change, or contrast. For the thinnest wafers, 750-5 and 751-3, the contrast was insufficient to clearly detect even the coarsest recorded grating.

For the finest gratings, the patterns are probably not recorded throughout the full thickness of the thickest wafers, being washed out by diffraction effects. However, this does not destroy the grating recorded in the region nearest the grating mask, and if this region is thick enough, readout is still possible.

2. $SrTiO_3$ (FIGURES C-7 THROUGH C-9)

While these wafers exhibit large photochromic optical density changes initially, the thermal decay is quite rapid. It is difficult, therefore, to both record the grating in the erase mode and read out the recorded grating photographically while appreciable contrast remains. Thus, for the thinnest wafer, ST-2-10, photographic readout of the recorded gratings was not achieved.

The photochromic coloration of these $SrTiO_3$ wafers is confined to a relatively thin surface layer which constitutes their effective thickness, regardless of actual thickness. Thus diffraction effects within the wafers are relatively unimportant. The resolution capabilities are thus affected by wafer thickness largely through crystal homogeneity.

3. $CaTiO_3$ (FIGURES C-10 THROUGH C-13)

These wafers exhibit higher photochromic contrast than those of either CaF_2 or $SrTiO_3$. Their photochromic thermal decay is about 10^2 times slower than that of $SrTiO_3$, but like $SrTiO_3$ their effective thickness is determined by the thin depth of photochromic coloration. Thus, resolution in these $CaTiO_3$ wafers is primarily limited by their poor optical quality. This difficulty is apparent in Figures C-10 through C-13 and is discussed in some detail in Section II.C. of this report.

VI. NEW TECHNOLOGY

No New Technology has been developed during this reporting period.

VII. SUMMARY AND CONCLUSIONS

We have carried out an extensive quantitative and comparative evaluation of a broad range of state-of-the-art inorganic photochromic materials which offer potential as information input planes for coherent optical data-processing applications. The evaluated samples comprise 17 wafers of various thicknesses of CaF_2:La,Na; CaF_2:Ce,Na; $SrTiO_3$:Ni,Mo,Al; and $CaTiO_3$:Ni,Mo. The range of wafer thicknesses included is 0.13 to 1.02 mm. The evaluation includes consideration of available wafer size and crystal quality, photochromic absorption spectra, quantitative erase mode sensitometry, time-intensity reciprocity, and resolution capabilities. Most of the evaluative tests were carried out in the erase mode, using coherent 5145 Å argon laser radiation. The results of these tests are presented and summarized in numerous graphs, tables, and photographs distributed throughout the text and in three appendices.

Some very general characteristics of the several materials evaluated are very briefly summarized below:

A. CaF_2 (WITH La,Na or Ce,Na Dopants)

1. Very high optical quality.
2. Moderately large wafer sizes available.
3. Long photochromic lifetime.
4. Excellent time-intensity reciprocity in the erase mode.
5. Relatively low erase mode sensitivity.
6. Low photochromic optical density per unit wafer thickness.
7. Moderate resolution capability, but at low contrast.

B. $SrTiO_3$:Ni,Mo,Al

1. Large wafer sizes available.
2. Moderate to good optical quality.
3. Relatively high erase mode sensitivity.
4. High photochromic optical density per unit wafer thickness.
5. Good resolution capability.
6. Short photochromic thermal lifetime.
7. Poor time-intensity reciprocity in the erase mode.

C. $CaTiO_3$:Ni,Mo

1. High photochromic optical density per unit wafer thickness.
2. Moderate photochromic thermal lifetime.
3. Good resolution capability, but seriously limited by poor optical quality.

4. Relatively poor time-intensity reciprocity in the erase mode.
5. Relatively low erase mode sensitivity.
6. Relatively small wafer sizes available.
7. Poor optical quality.

All of the wafers studied and evaluated are being forwarded to NASA under separate cover. For support, these wafers are mounted on 5 by 5-cm Al frames. (The cement used is Dow Sticky Wax; it is soluble in warm xylene).

VIII. ACKNOWLEDGMENTS

The author is pleased to acknowledge the very extensive and capable technical assistance of R. Infanti in the preparation and treatment of many sample wafers and in the performance of a number of experiments. Others who have contributed in various technical capacities include: G. Latham, R. Nielsen, and W. Prindle.

REFERENCES

1. R. C. Duncan, Ninth Progress Report, September 1970, Contract No. NAS 5-10335.
2. W. Phillips and R. C. Duncan, Metallurgical Trans. 2, 769 (1971).
3. B. W. Faughnan and Z. J. Kiss, Final Report, March 1969, Contract No. DASA-01-68-C-0064.
4. R. C. Duncan, Final Report, April 1969, Contract No. NAS 5-10335.
5. R. C. Duncan, Final Report, January 1970, Contract No. NAS 5-10335.
6. B. W. Faughnan and Z. J. Kiss, IEEE J. Quantum Electronics QE-5, 17 (1969).
7. L. Merker, J. American Ceramic Soc. 45, 366 (1962).
8. R. C. Duncan, Interim Report, April 1968, Contract No. NAS 5-10335.
9. J. J. Amodei, Ph.D. Thesis, University of Pennsylvania, 1968.
10. R. C. Duncan and Z. J. Kiss, Third Progress Report, October 1967, Contract No. NAS 5-10335.

APPENDIX A

This appendix comprises Figures A-1 through A-15 showing the photochromic absorption spectra of the first 15 sample wafers listed in Table 1 in Section II of this report. Each figure is labeled with the appropriate wafer identification number (in an abbreviated form in some cases) from that table. The order of the figures is the same as that of the wafers listed in Table I.

The solid curves in each figure (curve 1 in Figures A-1 through A-7) correspond to the unswitched or thermally stable photochromic states of the respective wafers. The broken curves (curve 2 in Figures A-1 through A-7) correspond to the saturated photochromic switched states of the respective wafers. The long-short dashed curves (curve 3 in Figures A-1 through A-7) correspond to the optically erased states of those wafers for which photochromic switching under the conditions of these experiments was not totally optically reversible. For these wafers, complete return to the switched state can only be achieved thermally at temperatures of about 100°C or greater.

For a description of the experimental procedures and a discussion of the data, see Section III of the text of this report.

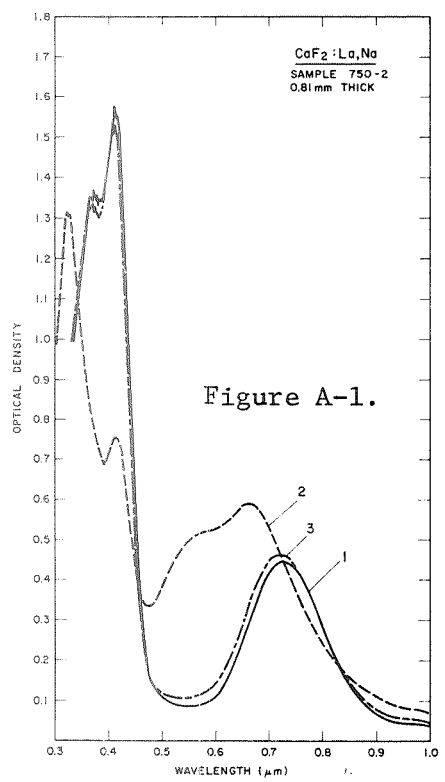

Figure A-1.

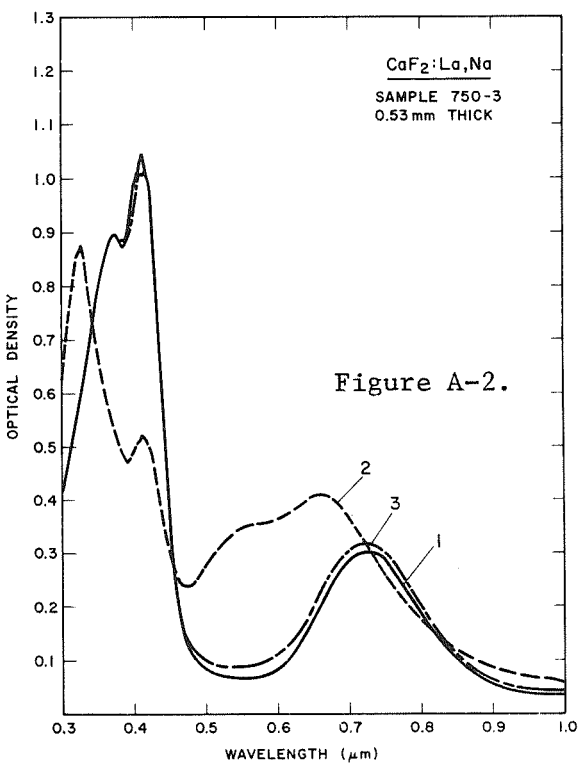

Figure A-2.

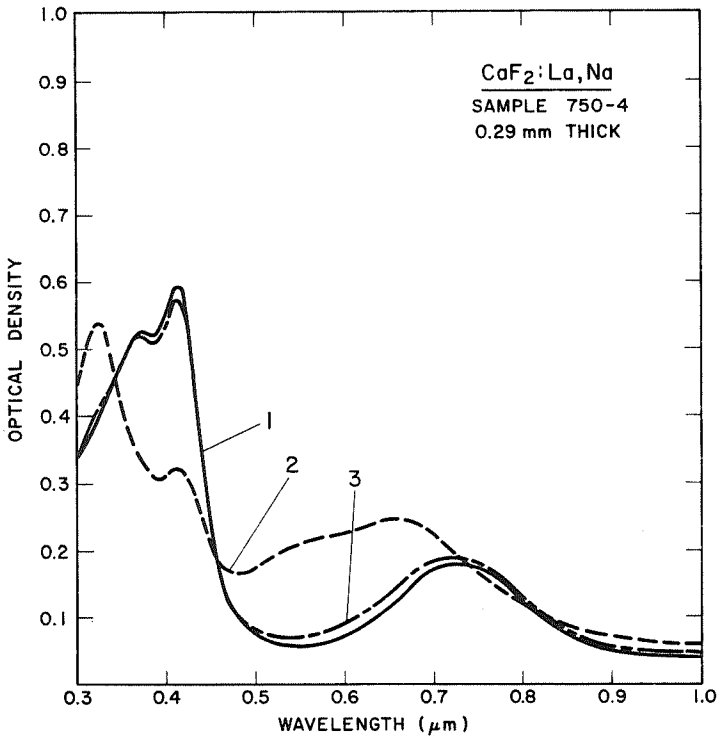

Figure A-3.

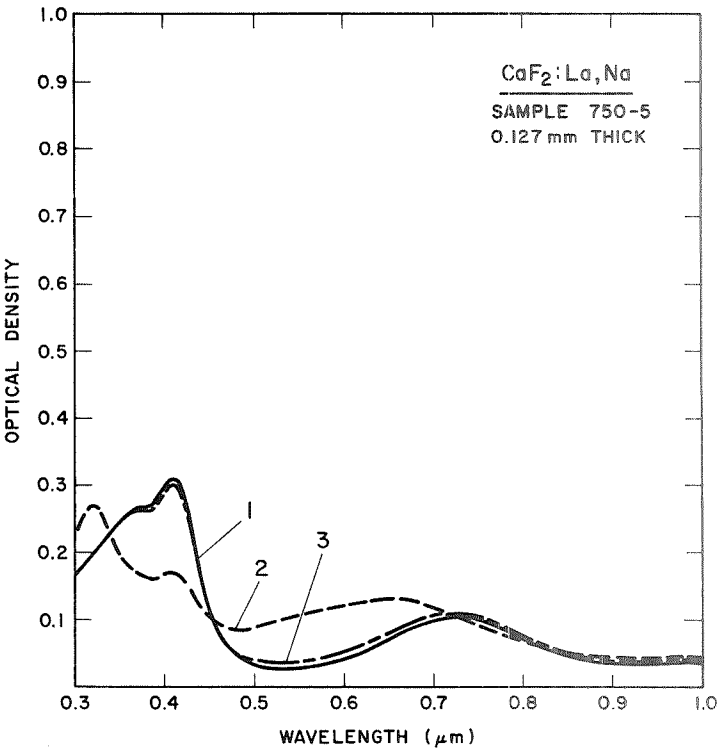

Figure A-4.

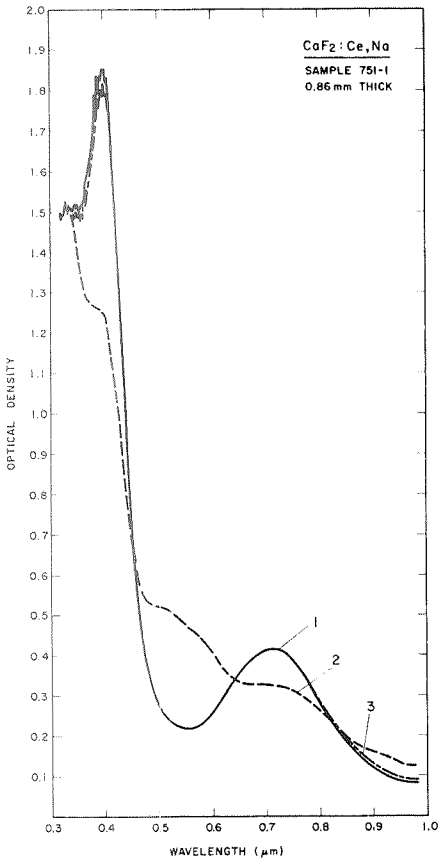

Figure A-5.

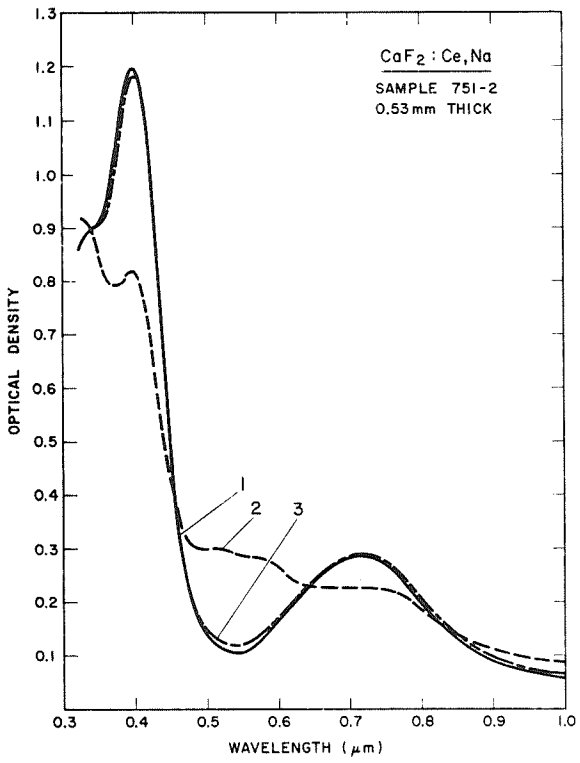

Figure A-6.

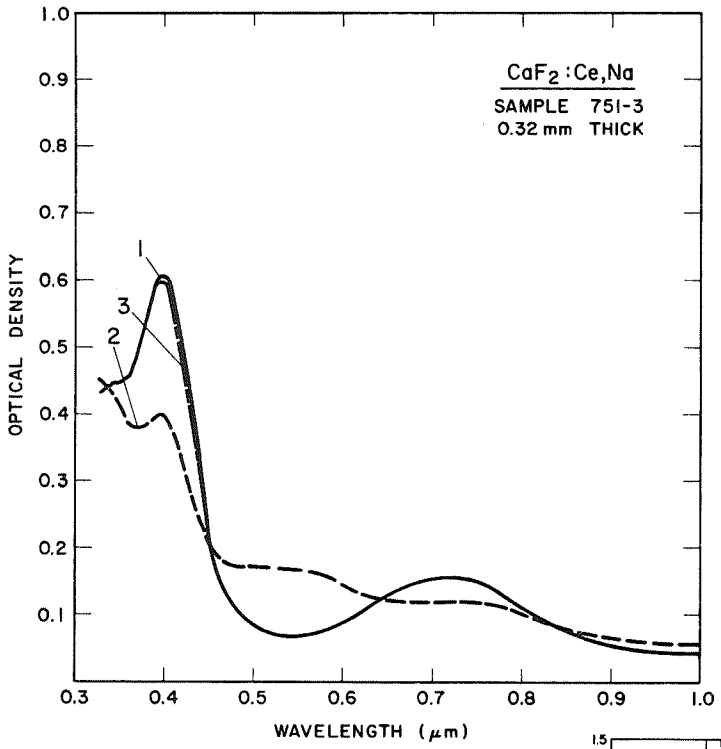

Figure A-7.

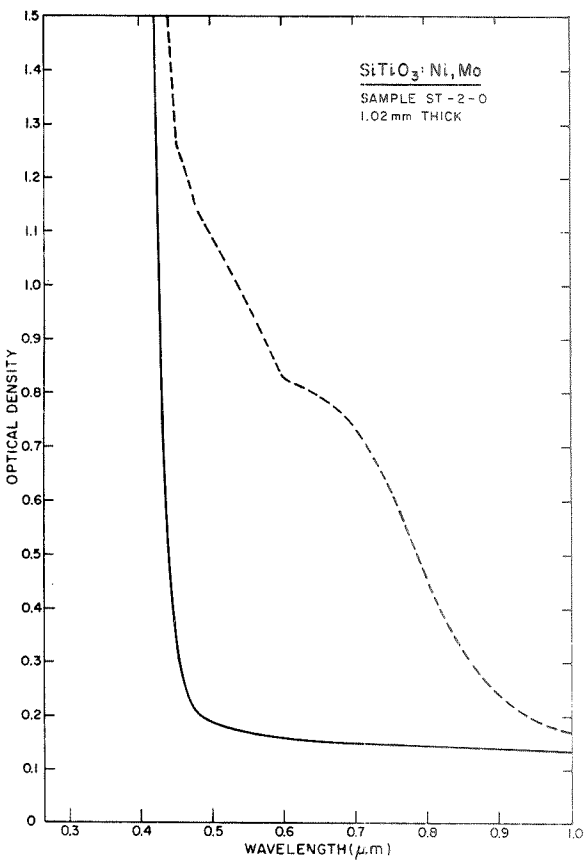

Figure A-8.

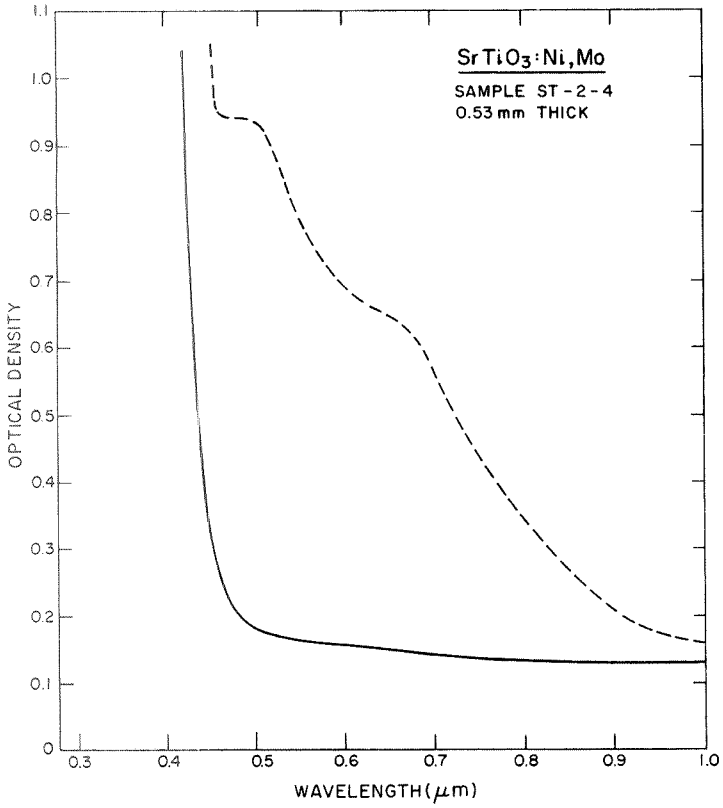

Figure A-9.

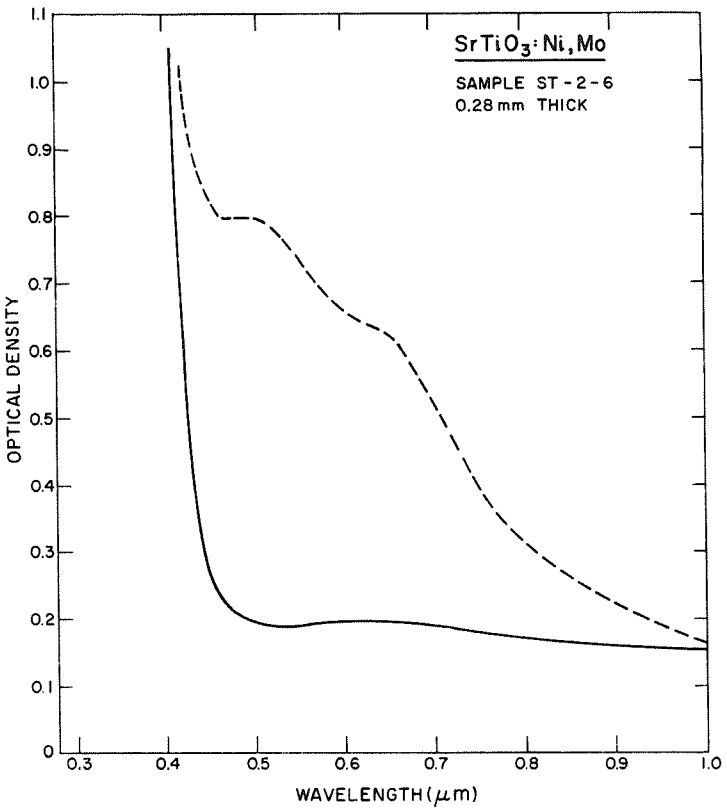

Figure A-10.

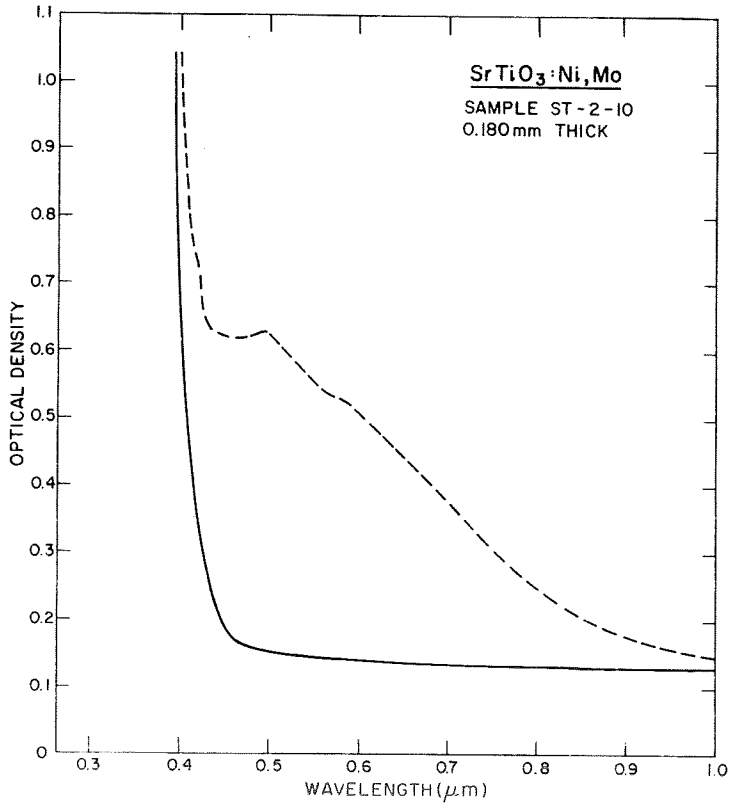

Figure A-11.

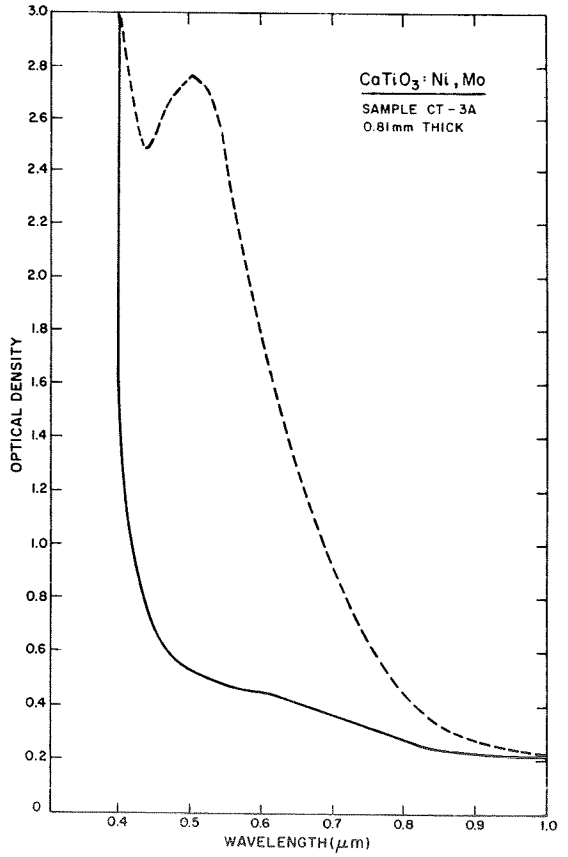

Figure A-12.

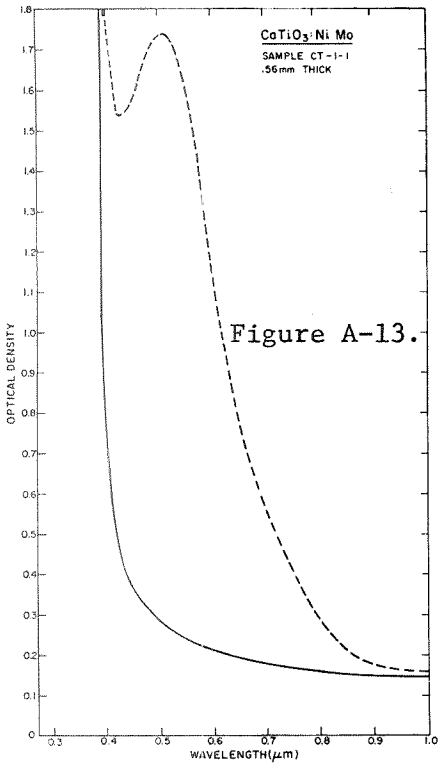

Figure A-13.

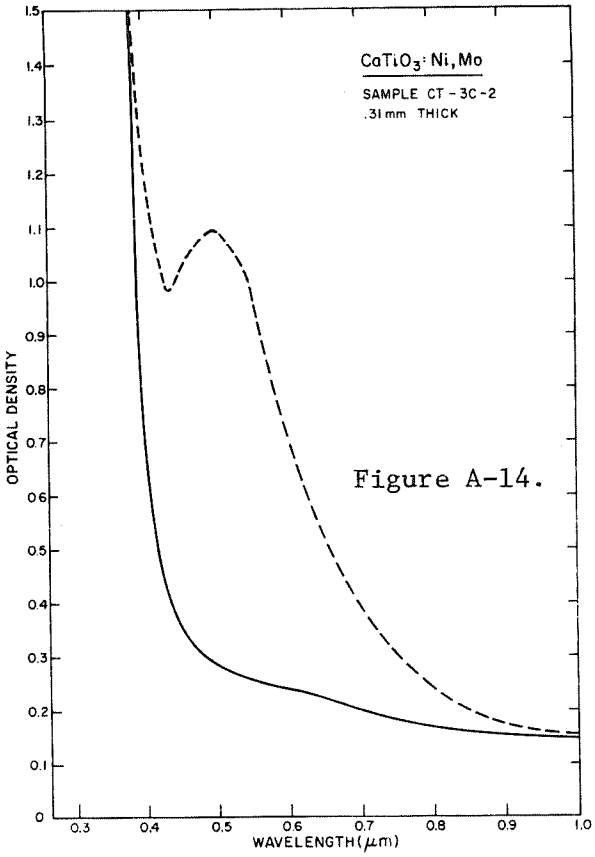

Figure A-14.

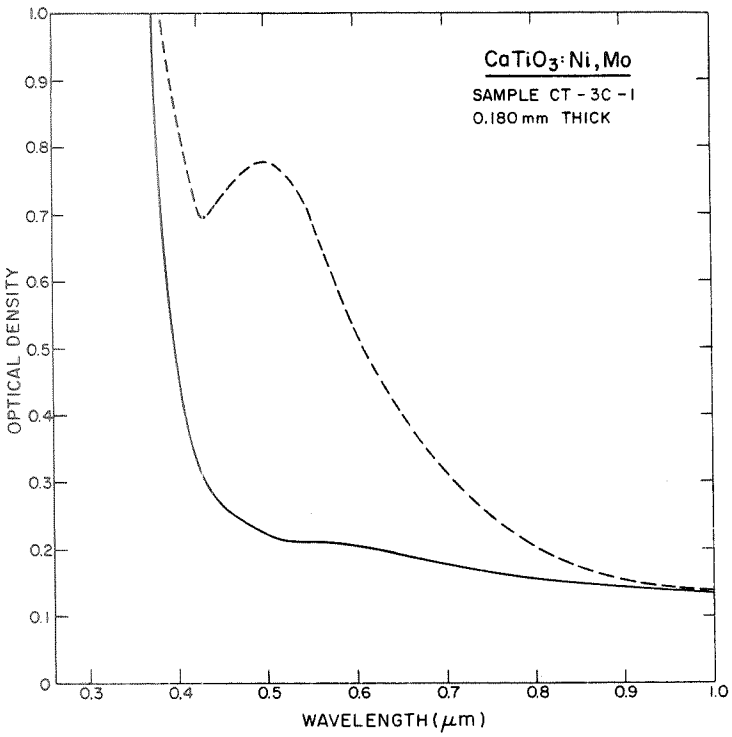

Figure A-15.

APPENDIX B

This appendix comprises Figures B-1 through B-15 showing families of erase mode sensitivity curves for the first 15 sample wafers listed in Table I in Section II of the text of this report. Each figure is labeled with the appropriate wafer identification number (in an abbreviated form in some cases) from that table. The order of the figures in this appendix is the same as that of the wafers listed in Table I.

The display format used for these curves, optical density change-versus the logarithm of the exposure, places major emphasis on the middle exposure range in which the greatest optical density changes occur, and corresponds to the standard format used for sensitometric data for photographic film. For each sample, the curves corresponding to various erase beam intensities are labeled with the measured beam power density in mW/cm^2.

For a description of the experimental procedures and a discussion of the data, see Section IV of this report.

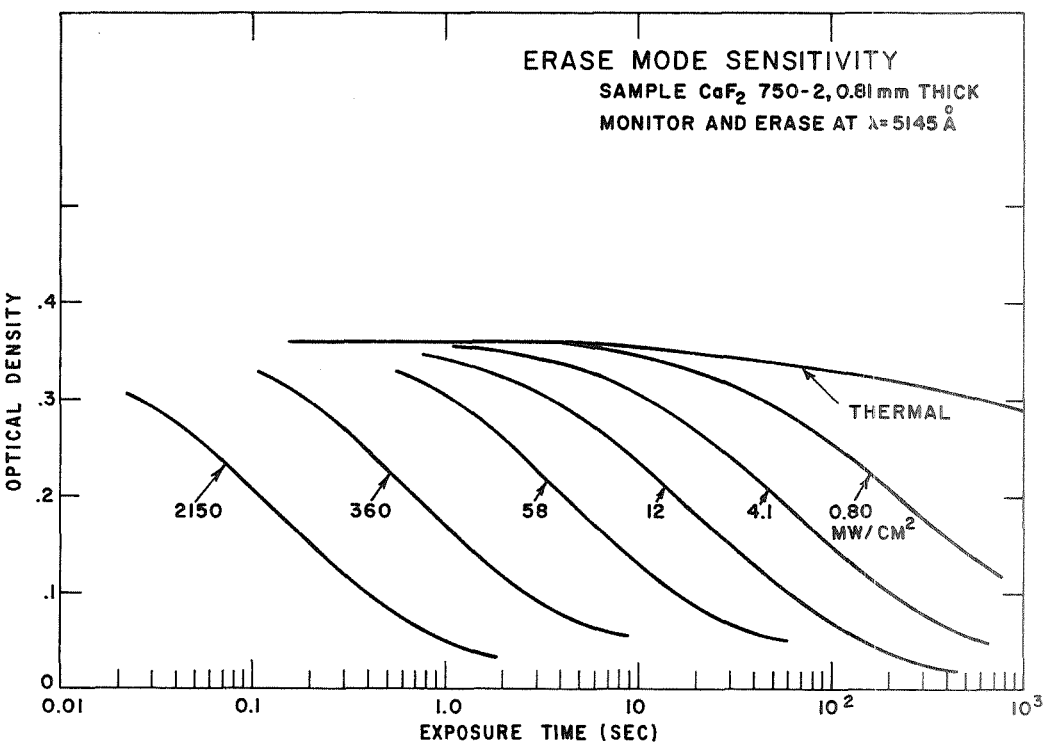

Figure B-1.

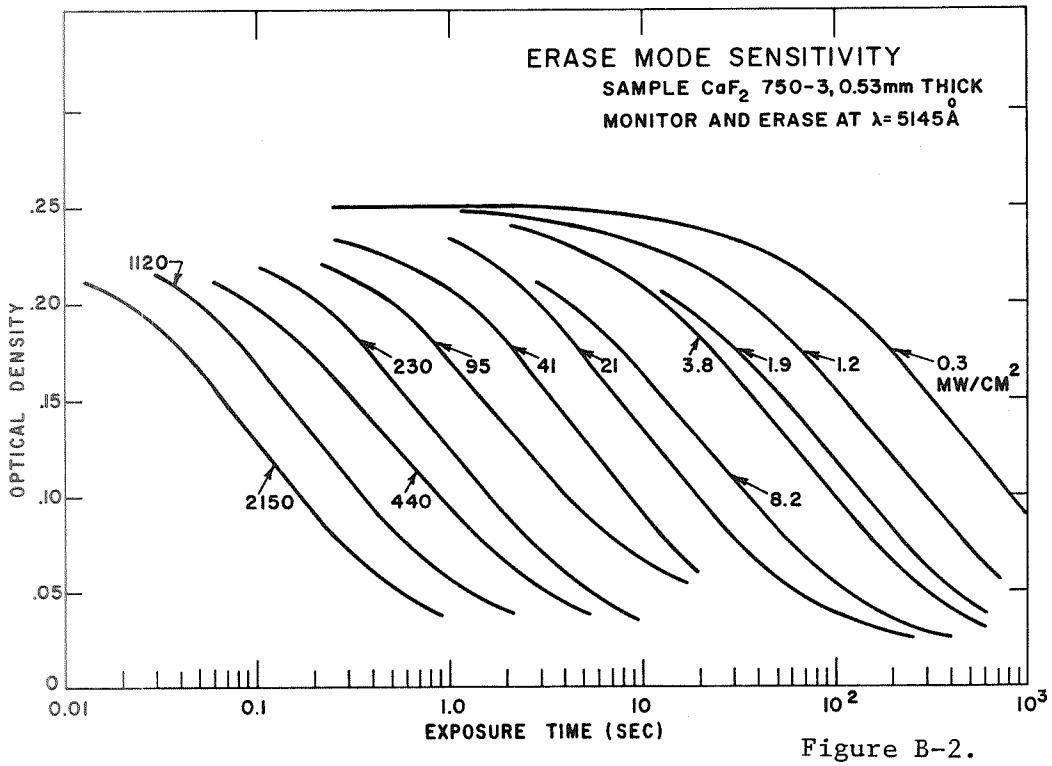

Figure B-2.

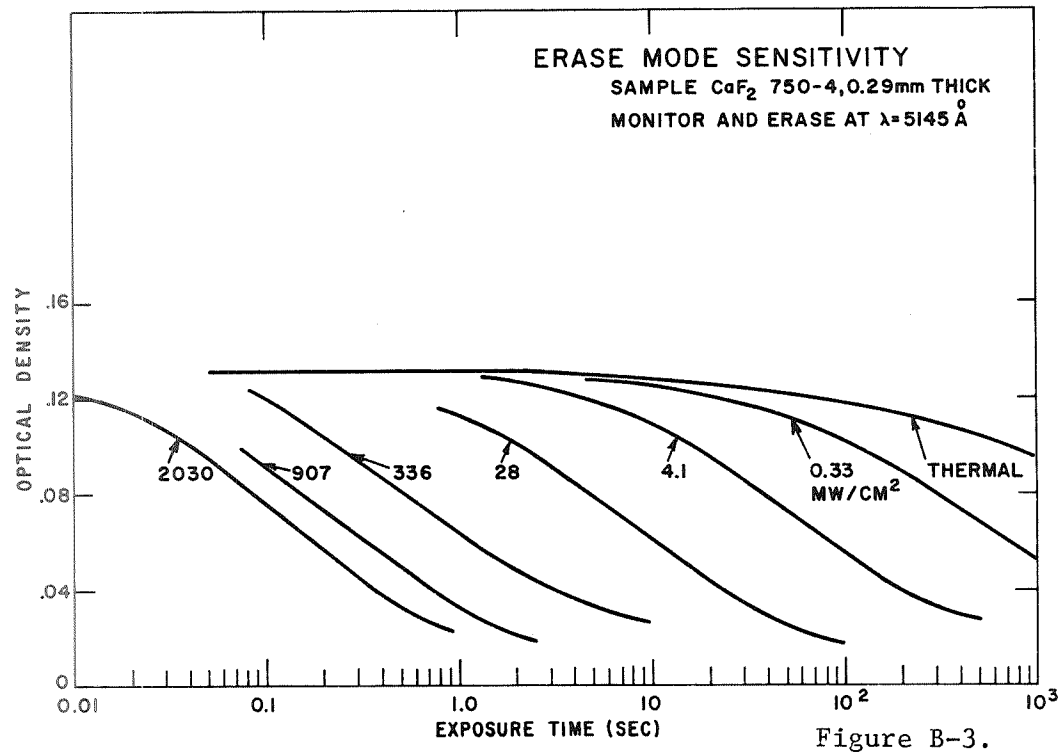

Figure B-3.

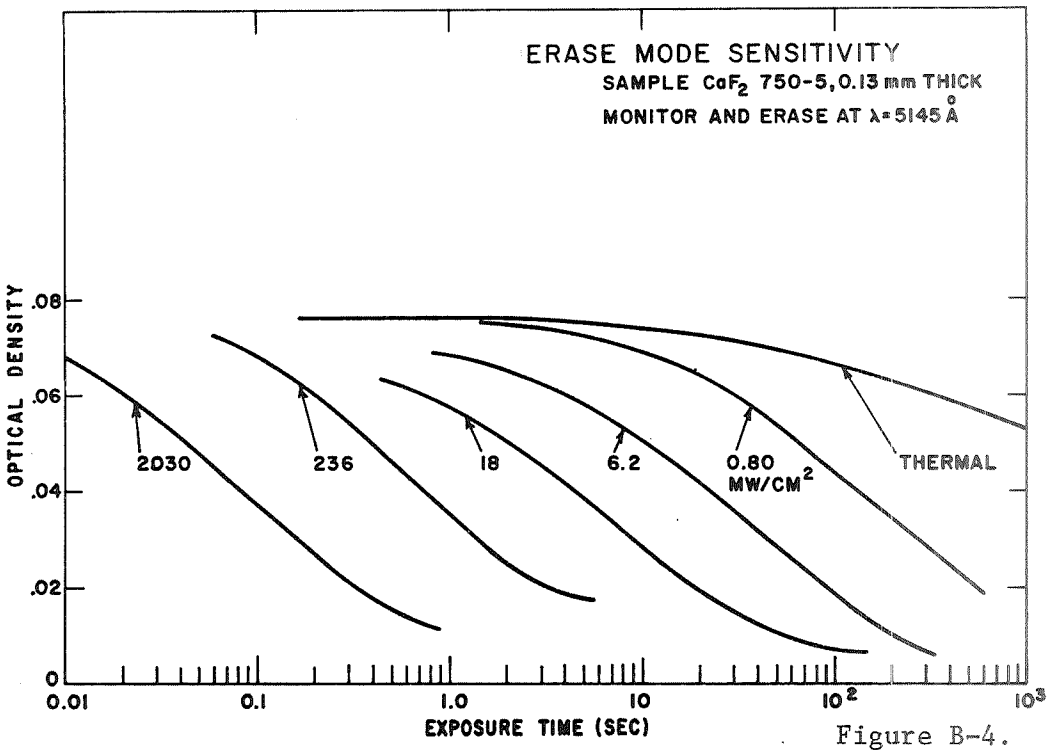

Figure B-4.

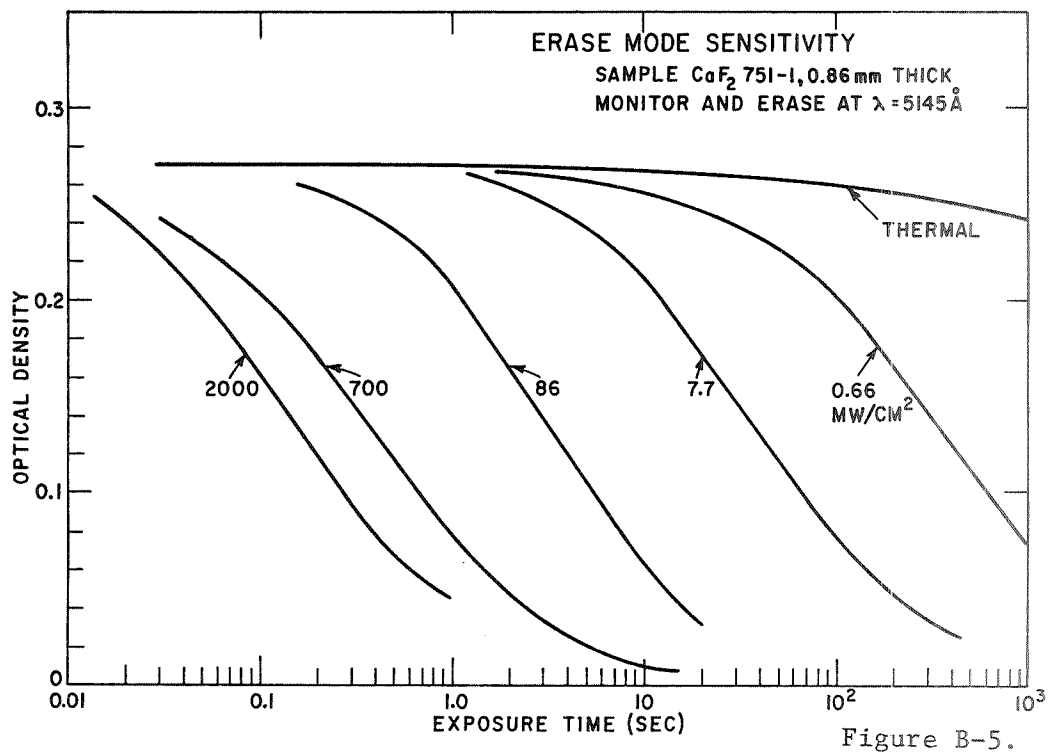

Figure B-5.

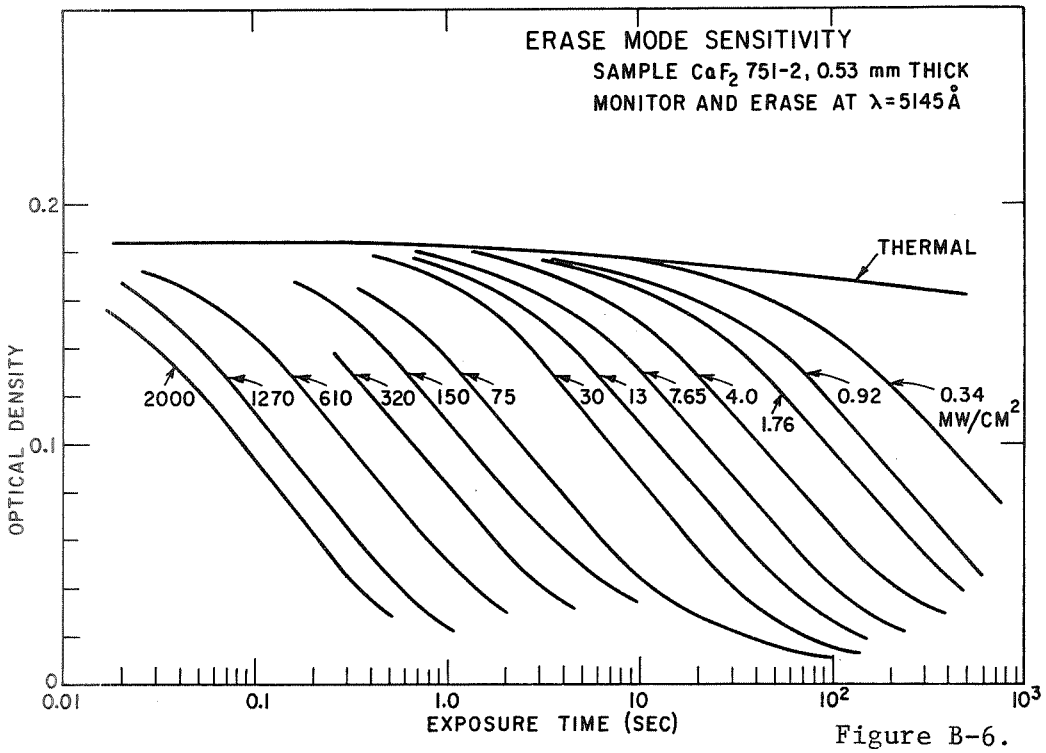

Figure B-6.

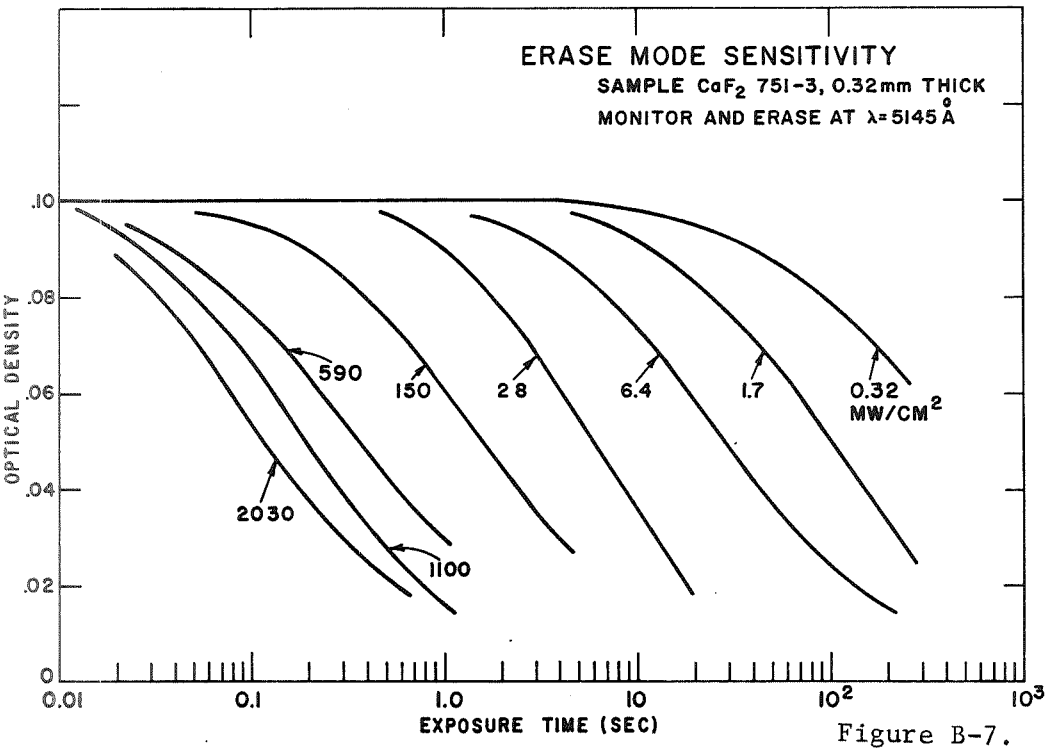

Figure B-7.

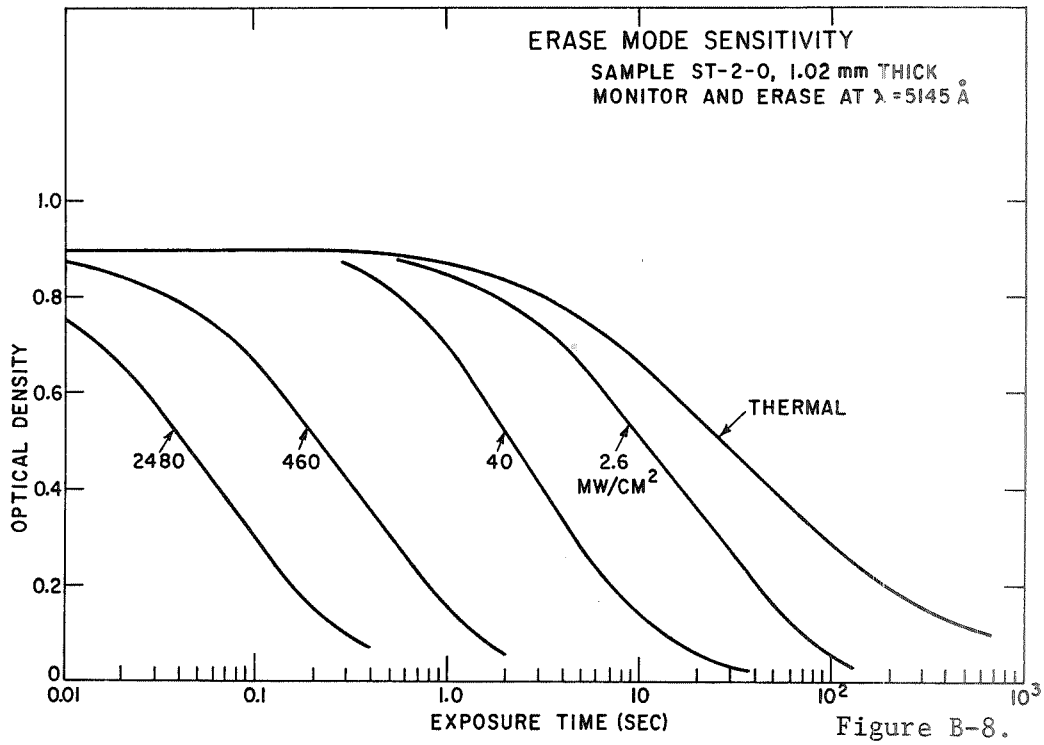

Figure B-8.

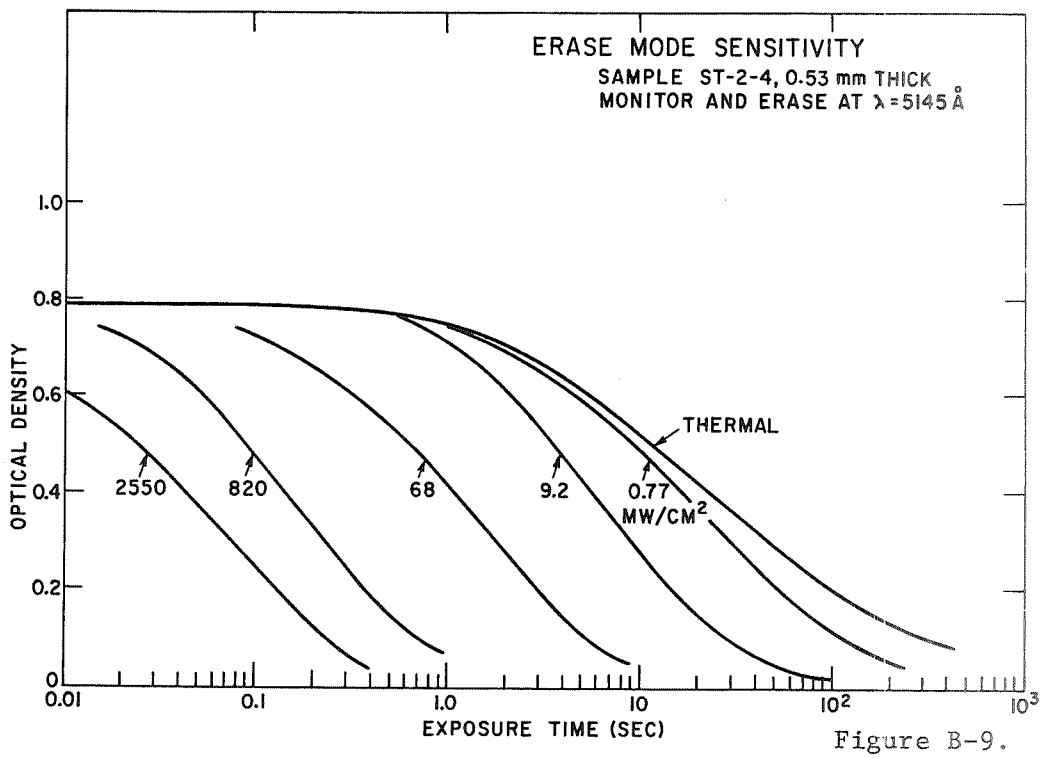

Figure B-9.

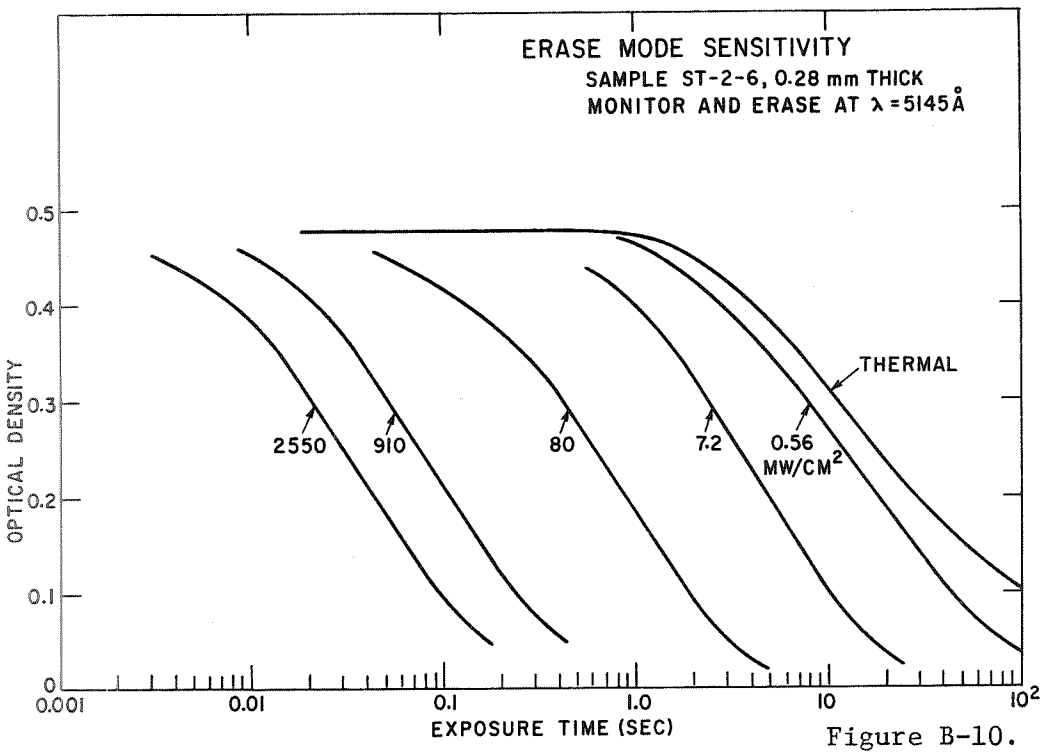

Figure B-10.

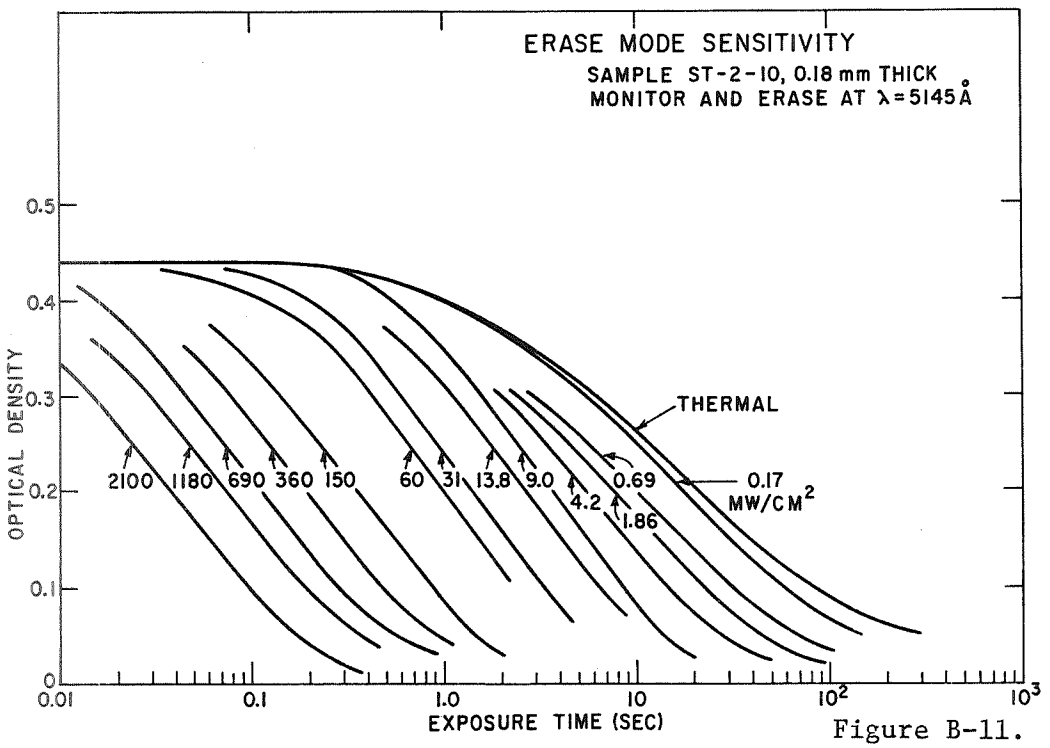

Figure B-11.

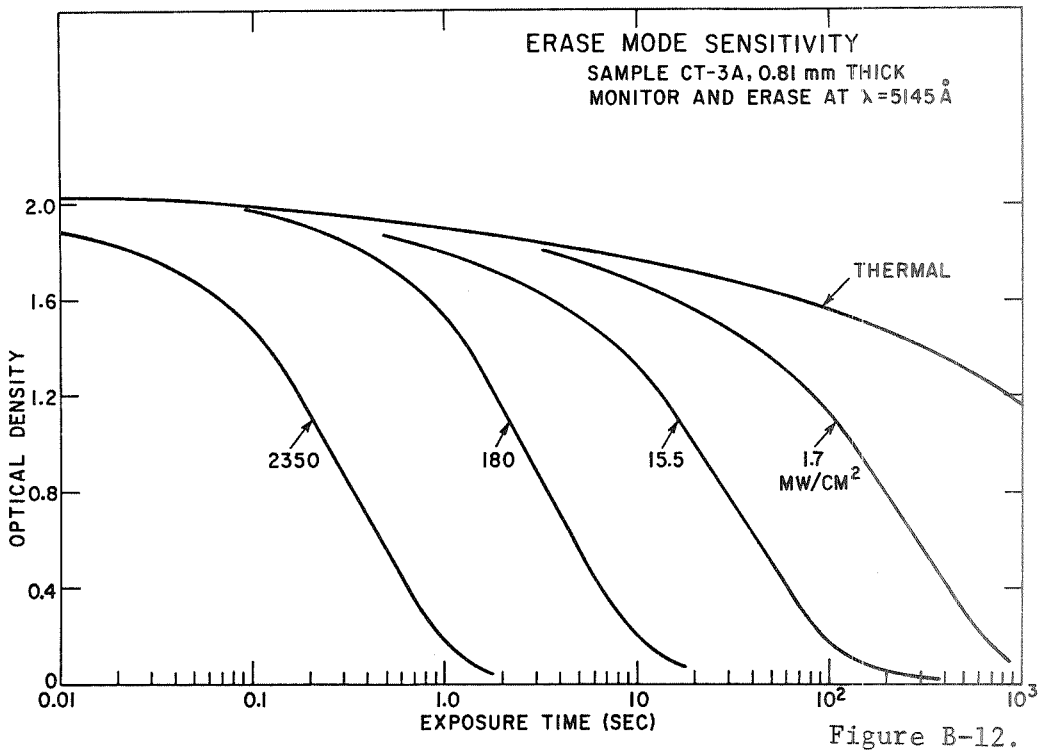

Figure B-12.

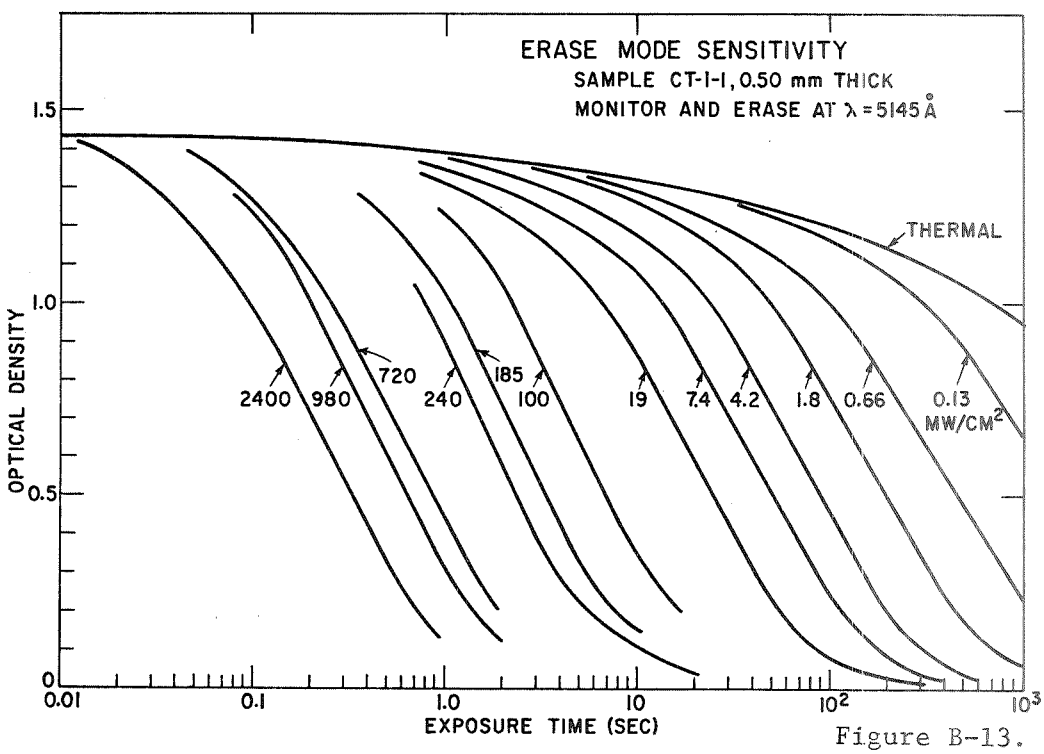

Figure B-13.

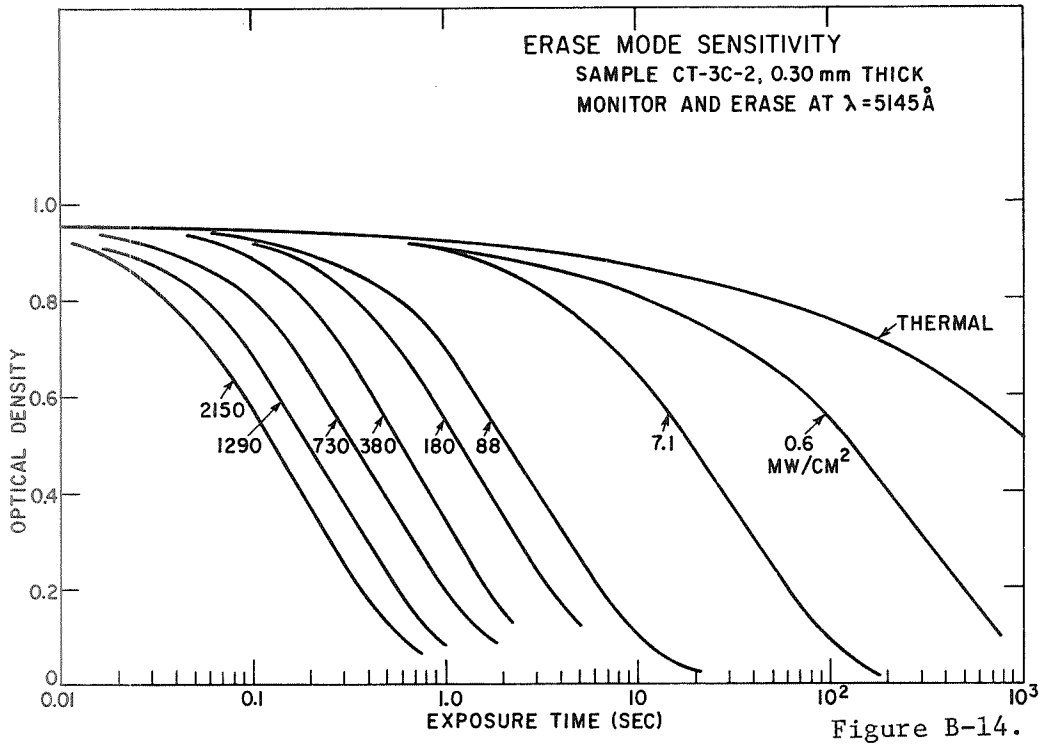

Figure B-14.

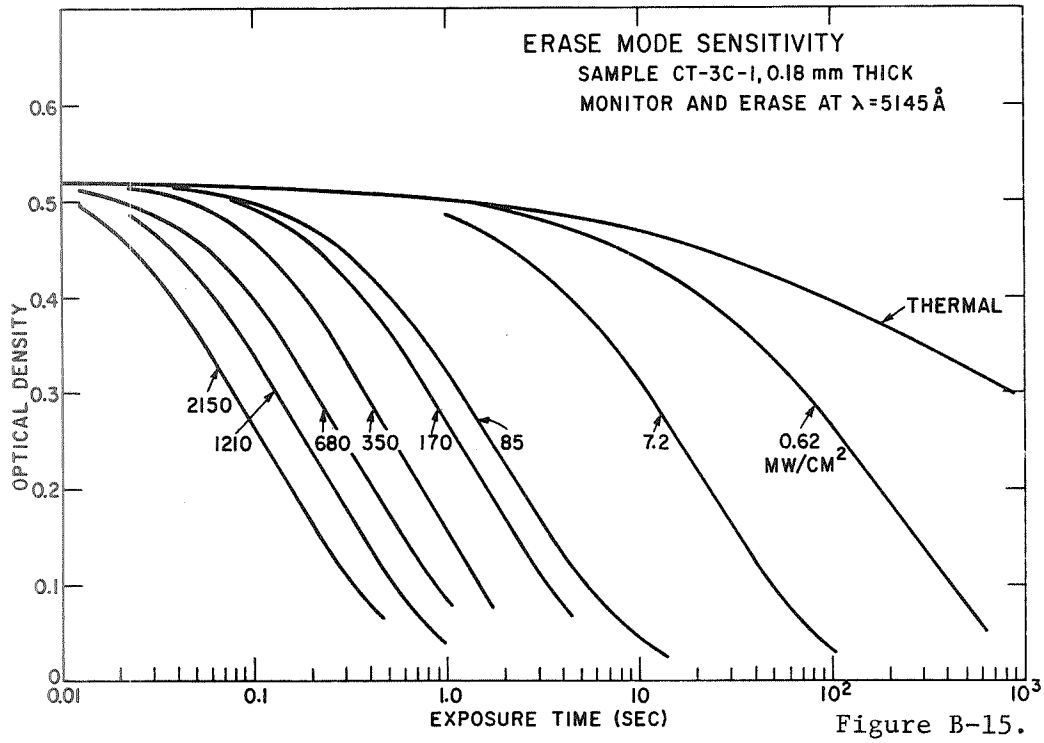

Figure B-15.

APPENDIX C

This appendix comprises Figures C-1 through C-13. Figure C-1 shows transmission photomicrographs of a set of line gratings with different grating spacings on high-contrast photographic film. The gratings were photographed in coherent 5145 Å light from an argon laser.

Figures C-2 through C-13 are similar transmission photomicrographs of those gratings as recorded by contact printing on photochromic sample wafers listed in Table I in Section II of the text of this report. Each figure is labeled with the appropriate wafer identification number (in an abbreviated form in some cases) from that table. The order of the figures is the same as that of the wafers listed in Table I, except that not all wafers listed there are included in this appendix. The gratings were both recorded and photographed in coherent 5145 Å light from an argon laser.

Master

25 ln. pr./mm

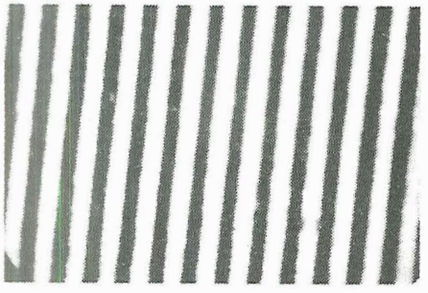

40 ln. pr./mm

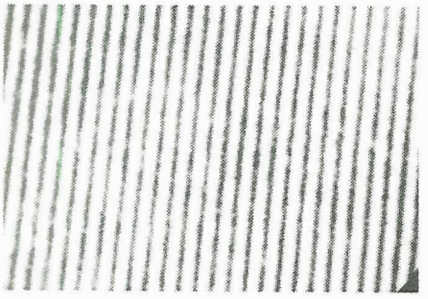

80 ln. pr./mm

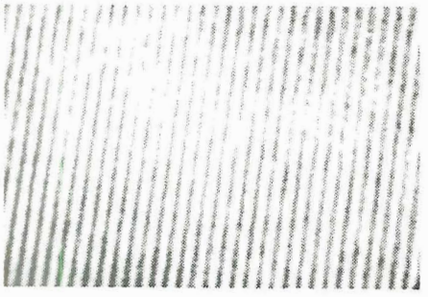

100 ln. pr./mm

Figure C-1

Wafer 750-2

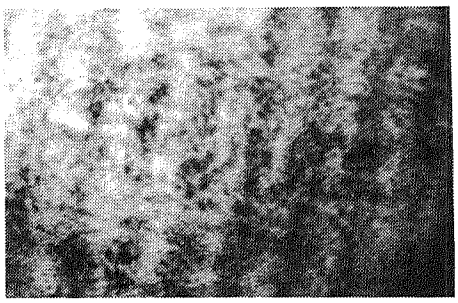

25 ln. pr./mm

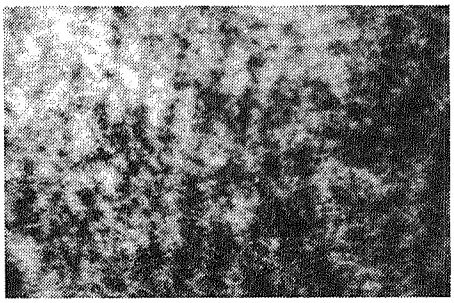

40 ln. pr./mm

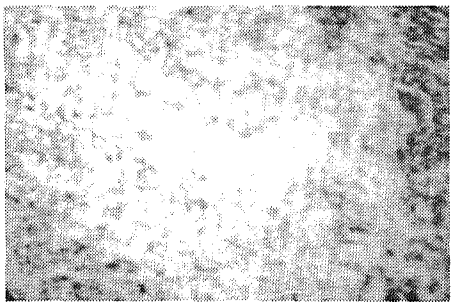

80 ln. pr./mm

Figure C-2

Wafer 750-3

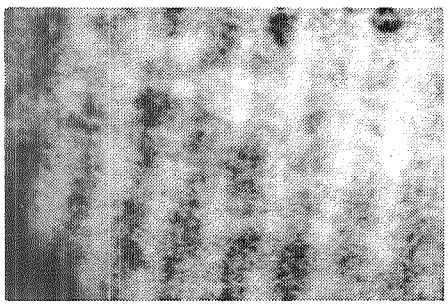

25 ln. pr./mm

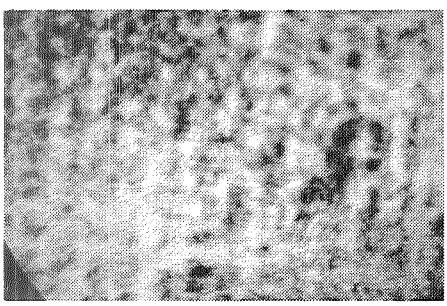

40 ln. pr./mm

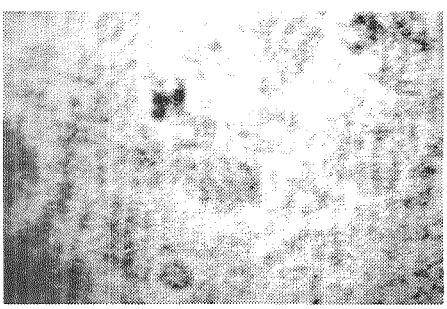

80 ln. pr./mm

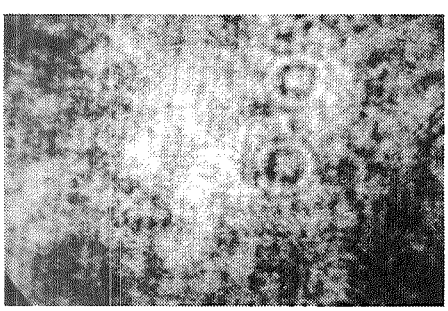

100 ln. pr./mm

Figure C-3

Wafer 750-4

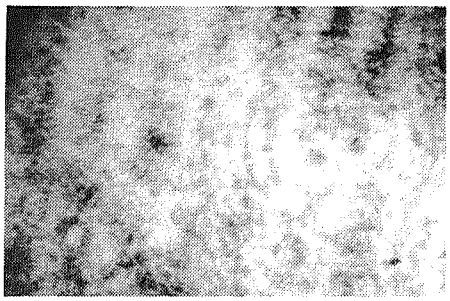

25 ln. pr./mm

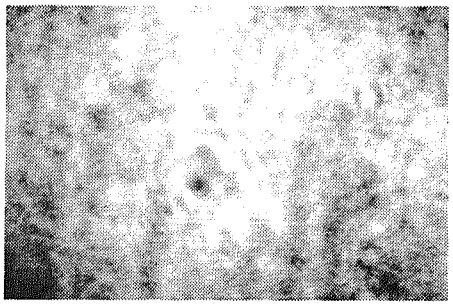

40 ln. pr./mm

Figure C-4

Wafer 751-1

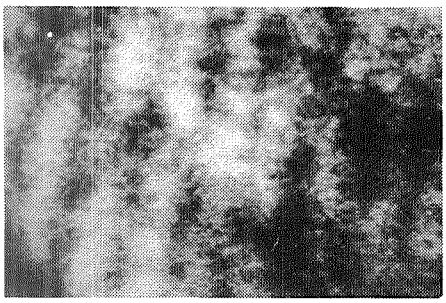

25 ln. pr./mm

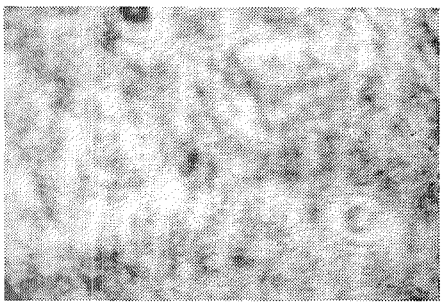

40 ln. pr./mm

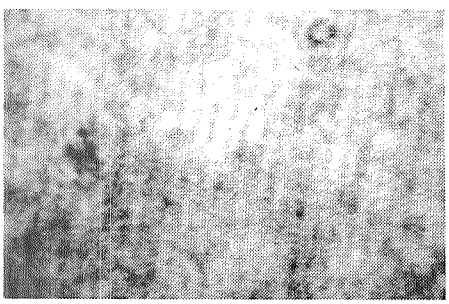

80 ln. pr./mm

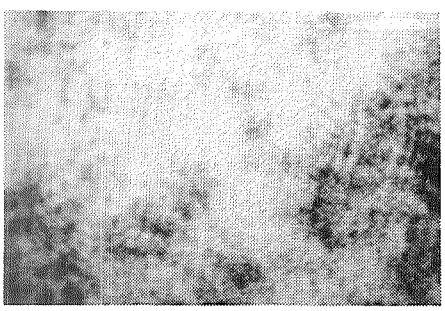

100 ln. pr./mm

Figure C-5

Wafer 751-2

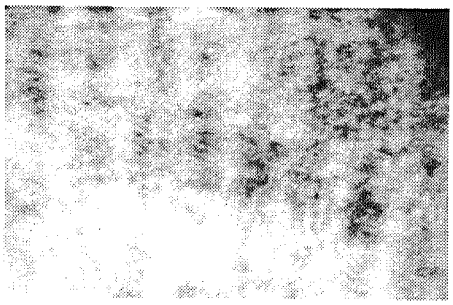

25 ln. pr./mm

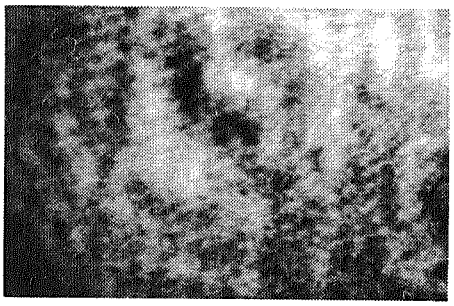

40 ln. pr./mm

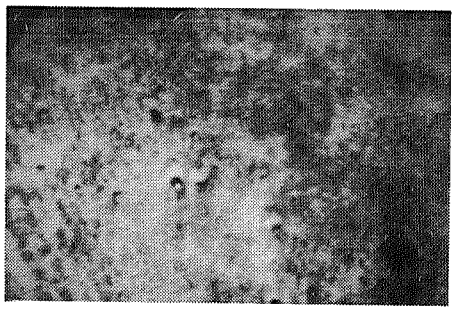

80 ln. pr./mm

Figure C-6

Wafer ST-2-0

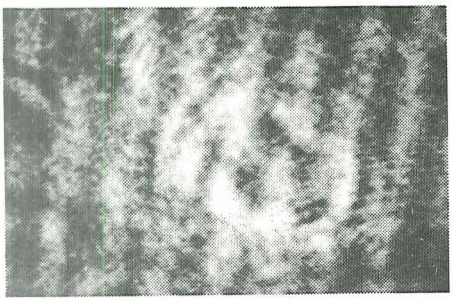

25 ln. pr./mm

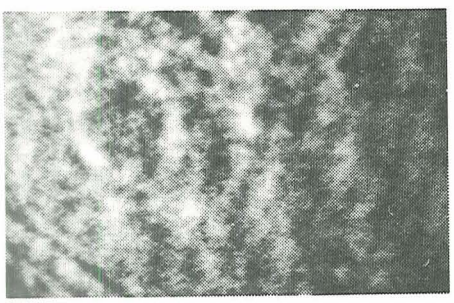

40 ln. pr./mm

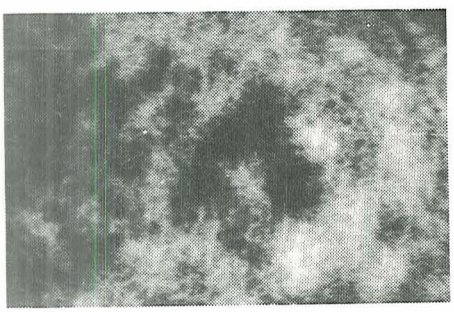

80 ln. pr./mm

Figure C-7

Wafer ST-2-4

25 ln. pr./mm

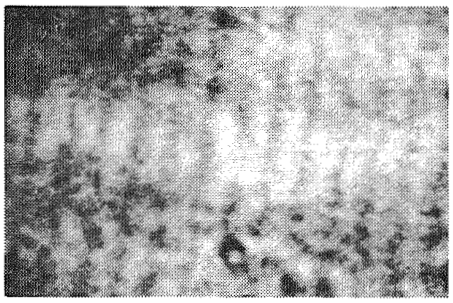

40 ln. pr./mm

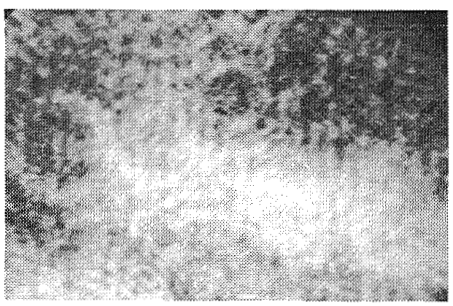

80 ln. pr./mm

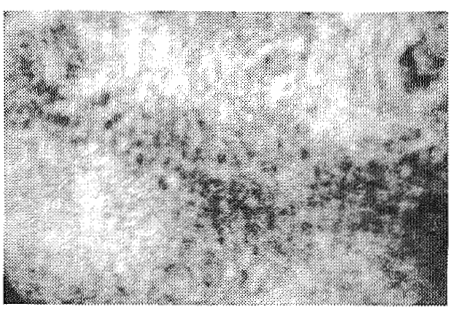

100 ln. pr./mm

Figure C-8

Wafer ST-2-6

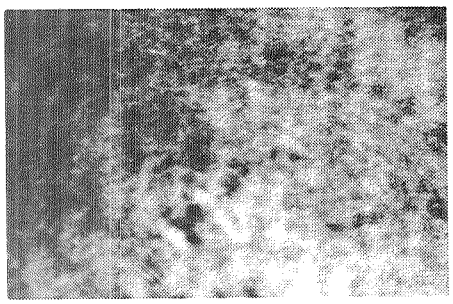

40 ln. pr./mm

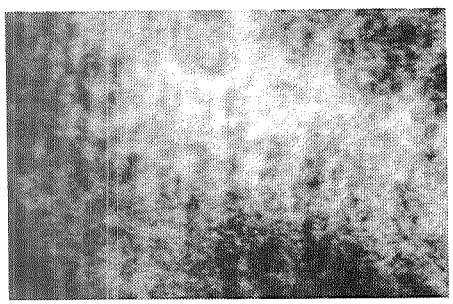

80 ln. pr./mm

Figure C-9

Wafer CT-3 A

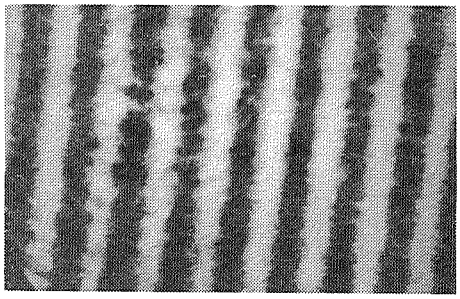

25 ln. pr./mm

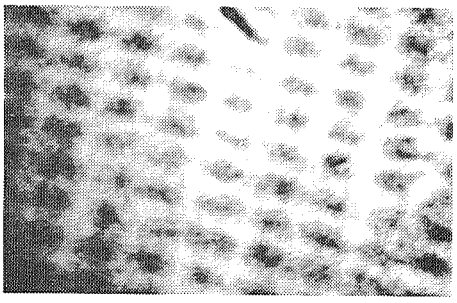

40 ln. pr./mm

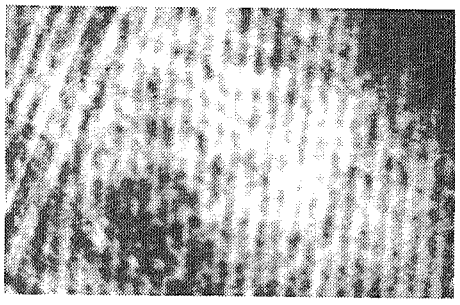

80 ln. pr./mm

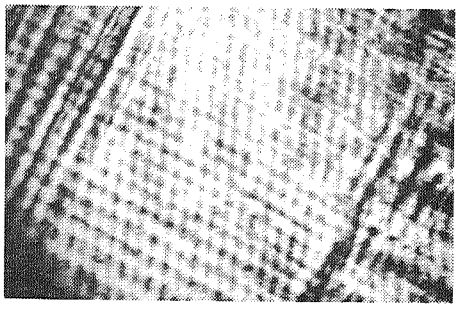

100 ln. pr./mm

Figure C-10

Wafer CT-1-1

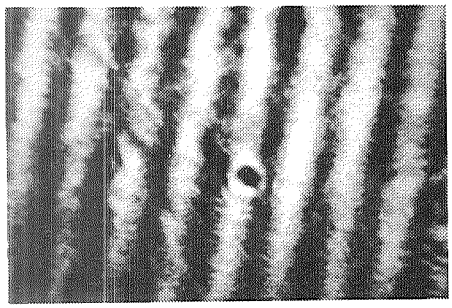

25 ln. pr./mm

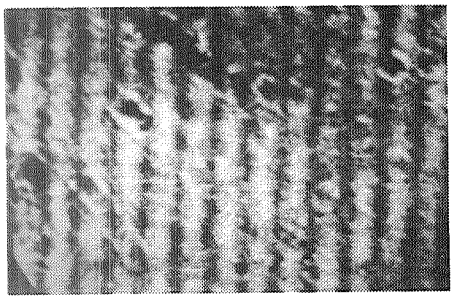

40 ln. pr./mm

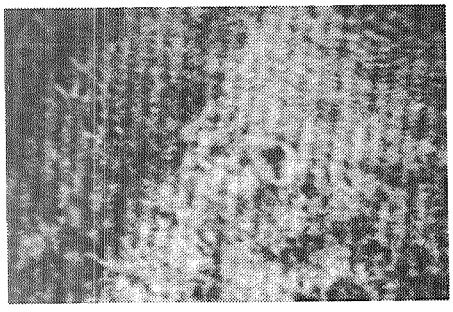

80 ln. pr./mm

Figure C-11

Wafer CT-3C-2

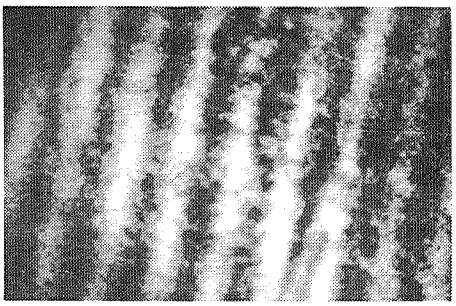

25 ln. pr./mm

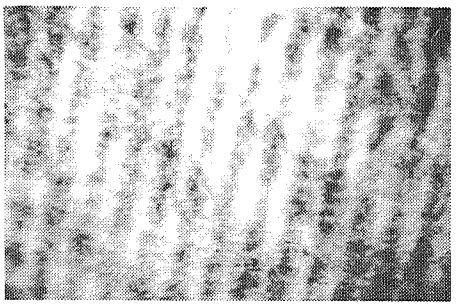

40 ln. pr./mm

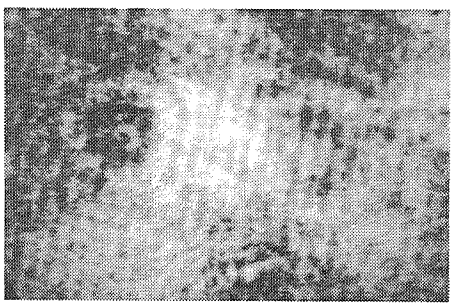

80 ln. pr./mm

100 ln. pr./mm

Figure C-12

Wafer CT-2C-D

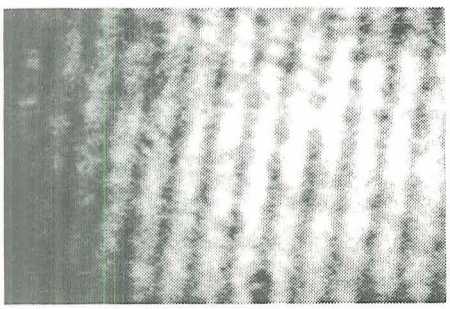

40 ln. pr./mm

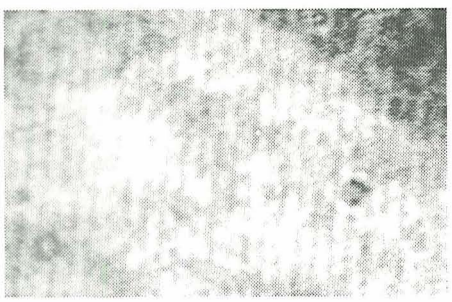

80 ln. pr./mm

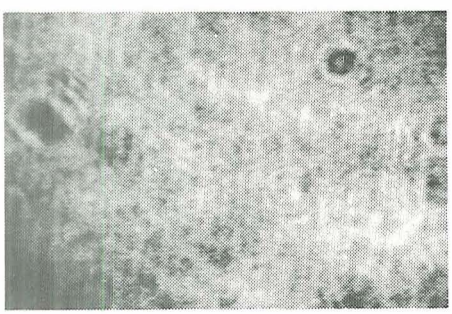

100 ln. pr./mm

Figure C-13